Inorganic Chemistry

Article

pubs.acs.org/IC

# An Integrated Approach (Thermodynamic, Structural, and Computational) to the Study of Complexation of Alkali-Metal Cations by a Lower-Rim Calix[4]arene Amide Derivative in Acetonitrile

Gordan Horvat,[†] Vladimir Stilinović,[†] Tomica Hrenar,[†] Branko Kaitner,[†] Leo Frkanec,[‡] and Vladislav Tomišić*[,†]

[†]Department of Chemistry, Faculty of Science, University of Zagreb, Horvatovac 102a, 10000 Zagreb, Croatia

[‡]Laboratory of Supramolecular and Nucleoside Chemistry, Department of Organic Chemistry and Biochemistry, Ruđer Bošković Institute, Bijenička c. 54, 10000 Zagreb, Croatia

Supporting Information

**ABSTRACT:** The calix[4]arene secondary-amide derivative **L** was synthesized, and its complexation with alkali-metal cations in acetonitrile (MeCN) was studied by means of spectrophotometric, NMR, conductometric, and microcalorimetric titrations at 25 °C. The stability constants of the 1:1 (metal/ligand) complexes determined by different methods were in excellent agreement. For the complexation of $M^+$ (M = Li, Na, K) with **L**, both enthalpic and entropic contributions were favorable, with their values and mutual relations being quite strongly dependent on the cation. The enthalpic and overall stability was the largest in the case of the sodium complex. Molecular and crystal structures of free **L**, its methanol and MeCN solvates, the sodium complex, and its MeCN solvate were determined by single-crystal X-ray diffraction. The inclusion of a MeCN molecule in the calixarene hydrophobic cavity was observed both in solution and in the solid state. This specific interaction was found to be stronger in the case of metal complexes compared to the free ligand because of the better preorganization of the hydrophobic *cone* to accept the solvent molecule. Density functional theory calculations showed that the flattened *cone* conformation ($C_2$ point group) of **L** was generally more favorable than the square *cone* conformation ($C_4$ point group). In the complex with $Na^+$, **L** was in square cone conformation, whereas in its adduct with MeCN, the conformation was slightly distorted from the full symmetry. These conformations were in agreement with those observed in the solid state. The classical molecular dynamics simulations indicated that the MeCN molecule enters the **L** hydrophobic cavity of both the free ligand and its alkali-metal complexes. The inclusion of MeCN in the *cone* of free **L** was accompanied by the conformational change from $C_2$ to $C_4$ symmetry. As in solution studies, in the case of $ML^+$ complexes, an allosteric effect was observed: the ligand was already in the appropriate square *cone* conformation to bind the solvent molecule, allowing it to more easily and faster enter the calixarene cavity.

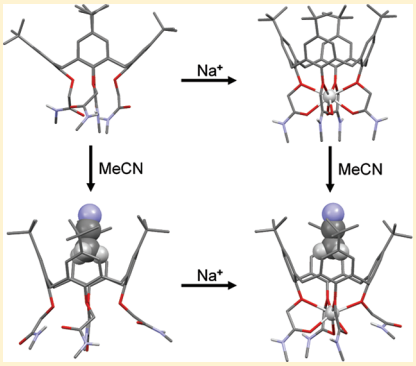


## INTRODUCTION

Calixarene derivatives have been extensively studied because of their ability to form inclusion complexes with a wide variety of guest species.[1] These macrocyclic receptors have been prepared by lower- and/or upper-rim functionalization of the parent calixarenes. By the appropriate choice of the substituents and the number of repeating phenolic units comprising the macrocycle, the efficient and, in some instances, selective binders of cations,[2] anions,[2b,3] and neutral molecules[2b,4] can be obtained.

The *p-tert*-butyl lower-rim-functionalized calix[4]arenes with carbonyl-containing substituents, which include calixarene ketones, esters, and amides, have been proven to be effective receptors for alkali, alkaline-earth, and transition-metal cations.[2c,d,f] An interesting feature of tetrasubstituted secondary-amide derivatives is the possibility of intramolecular NH···O═C hydrogen-bond formation. This was shown to have a strong influence on their binding abilities.[5] Besides the nature of the binding groups, the affinity of calixarenes toward metal cations strongly depends on the reaction medium, i.e., on the solvent used.[1d,5i,k,6] In this respect, the specific interactions of the ligand and the complex with the solvent molecules can be particularly important. Inclusion of an acetonitrile (MeCN) molecule in a calixarene hydrophobic cavity[4a−f,7] can serve as a striking example of such an interaction, which was shown to be synergetic with the binding of the cation in the ligand hydrophilic cavity.[5k,7a,8]

Even though the complexation reaction between the calixarene ligand (L) and the metal cation ($M^{z(M)}$; $z$(M) denotes the charge number) in solution (sln)

$$M^{z(M)}(sln) + L(sln) \rightleftarrows ML^{z(M)}(sln) \quad (1)$$

**Received:** March 2, 2012

   dx.doi.org/10.1021/ic300474s | *Inorg. Chem.* XXXX, XXX, XXX−XXX

seems rather simple, there are many processes and interactions that are involved in such a reaction and that determine its equilibrium. For that reason, in order to gain detailed insight into the reactions studied, it is advisible to employ a number of complementary experimental and computational techniques, so that one may support the other. In the present work, such an approach has been used in the investigation of the alkali-metal-cation complexation by a calix[4]arene secondary-amide derivative, namely, 5,11,17,23-tetra-*tert*-butyl-25,26,27,28-tetrakis(*N*-hexylcarbamoylmethoxy)calix[4]arene (**L**, Scheme 1) in MeCN. The goal was to address as many processes/

**Scheme 1. Synthesis of Compound L**[a]

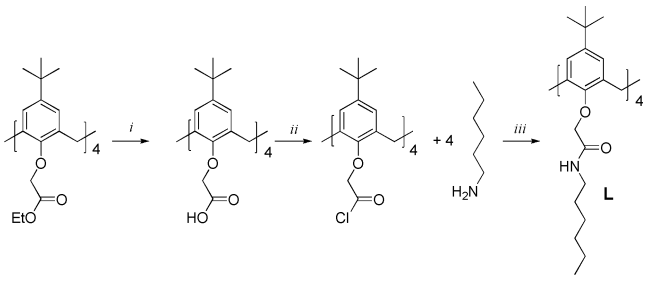


[a]Reagents and conditions: (i) NaOH, EtOH/$H_2O$; (ii) $SOCl_2$; (iii) $Et_3N$, dry $CH_2Cl_2$, Ar.

interactions involved in the complexation reaction as possible from both thermodynamic and structural points of view. In line with this, detailed spectrophotometric, NMR, electrochemical, and microcalorimetric investigations were carried out, along with the X-ray solid-state structure determinations of the free ligand and its complexes. Particular attention was focused on the formation of the **L**MeCN adduct and the ternary M**L**MeCN$^+$ complexes (M denotes alkali metal). To the best of our knowledge, for the first time, the equilibrium constants for binding of the MeCN molecule with free calixarene and its metal-ion complex in a MeCN solution were estimated. In addition, the microscopic equilibrium constants for the formation of Li**L**$^+$ and Li**L**MeCN$^+$ complex species were assessed. To shed more light on the complexation properties and structures of the species involved, classical molecular dynamics (MD) and quantum-chemical computations were also performed. Among other things, these studies provided corroborations of the conclusions made on the basis of the experimental results.

## EXPERIMENTAL SECTION

**Synthesis.** All reagents were of the best grade commercially available and were used without further purification. Solvents were purified by standard procedures.[9] The acid chloride of calix[4]arene tetracetic acid (the *cone* conformer) was prepared as described in the literature.[10] Analytical thin-layer chromatography was performed on silica gel plates ($SiO_2$, Merck 60 $F_{254}$). Melting points were determined on a Kofler hot-bench apparatus and were not corrected. $^1$H and $^{13}$C NMR spectra were recorded with a Bruker Avance 300 or 600 MHz spectrometer ($\delta$ in ppm relative to $(CH_3)_4Si$ as an internal standard, $J$ values are in hertz). IR spectra were recorded by means of an ABB Bomem MB102 FTIR spectrometer. Mass spectrometry (MS) measurements were conducted on an Agilent 6410 Triple-Quadrupole mass spectrometer. Elemental analysis (C, H, and N) was provided by the Analytical Services Laboratory of the Rudjer Bošković Institute, Zagreb, Croatia.

*5,11,17,23-Tetra-tert-butyl-25,26,27,28-tetrakis(N-hexylcarbamoylmethoxy)calix[4]arene (**L**).* (a) *n*-Hexylamine (0.48 g, 2.24 mmol) and triethylamine (0.36 mL, 2.61 mmol) were added to the cooled (0 °C) dry $CH_2Cl_2$ (20 mL) under argon. Then, the acid chloride of calix[4]arene tetracetic acid (the *cone* conformer)[10] (0.45 g, 0.47 mmol) in dry $CH_2Cl_2$ (10 mL) was added at once with a syringe. The reaction mixture was allowed to warm to room temperature and stirred overnight. After filtration, the filtrate was washed with NaOH (1.0 mol dm$^{-3}$), hydrochloric acid (1.0 mol dm$^{-3}$), brine, and water. After drying ($MgSO_4$) and evaporation of the solvent, the crude product was crystallized from $CH_2Cl_2$/petroleum ether. Recrystallization from methanol (MeOH) gave **L** (0.49 g, 71%) as white crystals. Mp: 233−234 °C. $R_f$ = 0.44 (5% MeOH/$CH_2Cl_2$).

$^1$H NMR (600 MHz, $CDCl_3$, 25 °C, TMS): $\delta$ 7.46 (4 H, t, $J$ = 5.82, NH), 6.77 (8 H, s, ArH), 4.47 (4 H, d, $J$ = 12.9, $ArCH_2Ar$), 4.47 (8 H, s, $OCH_2CO$), 3.37−3.33 (8 H, m, $CH_2NH$), 3.23 (4 H, d, $J$ = 13.0, $ArCH_2Ar$), 1.59−1.55 (8 H, m, $CH_2CH_2NH$), 1.35−1.28 (24 H, m, $CH_2CH_2CH_2$), 1.08 (36 H, s, $C(CH_3)_3$), 0.89 (12 H, t, $J$ = 6.8, $CH_3$).

$^{13}$C NMR (75 MHz, $CDCl_3$, 25 °C): $\delta$ 169.50 (C═O), 152.95 (ArC−O), 145.75 (*p*-ArC), 132.69 (*m*-ArC), 125.80 (*o*-ArC), 74.63 ($OCH_2CO$), 39.59 ($NHCH_2$), 33.88 (C-*tert*-butyl), 31.60 ($ArCH_2Ar$), 31.49 ($NCH_2CH_2$), 31.32 ($CH_3$-*tert*-butyl), 29.74 ($CH_2CH_2CH_2CH_3$), 26.81 ($CH_2CH_2CH_2CH_3$), 22.65 ($CH_2CH_3$), 14.05 ($CH_3$).

FTIR (KBr pellet): $\nu_{max}$/cm$^{-1}$ 3289 (s, NH), 3088 (w, Ar−H), 1654 (CONH, amide I), 1545 (CONH, amide II), 1362 (w, *tert*-butyl), 1195 (s, COC).

Elem anal. Calcd for $C_{76}H_{116}N_4O_8$ (1213.76): C, 75.21; H, 9.63; N, 4.62. Found: C, 74.90; H, 9.37; N, 4.32.

MS: $m/z$ 1213.9 [(M + H)$^+$]. Calcd for $C_{76}H_{117}N_4O_8^+$: $m/z$ 1213.9, 1235.8 [(M + Na)$^+$]. Calcd for $C_{76}H_{116}N_4O_8Na^+$: $m/z$ 1235.9.

(b) Preparation of compound **L** by aminolysis: To 100 mL of absolute MeOH were added 1 mmol of the calix[4]arene ethyl ester and 32 mmol of *n*-hexylamine. The mixture was kept for several weeks at room temperature. Colorless transparent needles of a MeOH solvate of **L** crystallized from the solution. The crystals were separated from the mother liquor by suction filtration, washed with MeOH, and dried to obtain a white powder, which was pure compound **L** (yield 54%). The spectroscopic data of the prepared compound were identical with those described above.

**Materials for Physicochemical Measurements.** The salts used for the investigation of **L** complexation were $LiClO_4$ (Fluka, p.a., and Sigma Aldrich, 99.99%), $NaClO_4·H_2O$ (Fluka p.a.), $NaClO_4$ (Sigma Aldrich, 98+%), $KClO_4$ (Merck, p.a.), $CsNO_3$ (Sigma, 99.5%), and $RbNO_3$ (Sigma, 99.7%). The solvent, acetonitrile (MeCN; Merck, Uvasol), was used without further purification. In most spectrophotometric and in all potentiometric titrations, the ionic strength was kept constant by the addition of $Et_4NClO_4$ (Fluka, p.a.).

**Spectrophotometry.** UV titrations were performed at 25.0 ± 0.1 °C by means of a Varian Cary 5 double-beam spectrophotometer equipped with a thermostatting device. The spectral changes of the **L** solution ($V_0$ = 2.0 cm$^3$, $c_0$ = 2.40 × 10$^{-4}$−2.46 × 10$^{-4}$ mol dm$^{-3}$, and $I_c$ = 0.01 mol dm$^{-3}$) were recorded upon the stepwise addition of an alkali-metal salt solution ($c$ = 9.59 × 10$^{-4}$−3.88 × 10$^{-3}$ mol dm$^{-3}$ and $I_c$ = 0.01 mol dm$^{-3}$) directly into the measuring cell of 1 cm path length (Hellma, Suprasil QX). Absorbances were sampled at 1 nm intervals, with an integration time of 0.2 s. Titrations for each M$^+$/**L** system were done in triplicate. The obtained spectrophotometric data were processed using the *SPECFIT* program.[11]

**Potentiometry.** The stability constant of the Na**L**$^+$ complex in MeCN was determined by the potentiometric titration of a 30.3 cm$^3$ $NaClO_4$ solution ($c_0$ = 1.0 × 10$^{-4}$ mol dm$^{-3}$) with a solution of **L** ($c$ = 7.34 × 10$^{-4}$ mol dm$^{-3}$) in a thermostatted titration vessel ($t$ = 25.0 ± 0.1 °C). The ionic strength of both solutions was set to 0.01 mol dm$^{-3}$ by $Et_4NClO_4$. The indicator electrode was a sodium-selective glass electrode (Metrohm, 6.0501.100) with an Ag/AgCl reference electrode (Metrohm, 6.0733.100) filled with a MeCN solution of $Et_4NCl$ ($c$ = 0.01 mol dm$^{-3}$). The working and reference half-cells were connected with a salt bridge containing 0.01 mol dm$^{-3}$ $Et_4NClO_4$. A Metrohm 713 pH meter was used for electromotivity measurements. The cell was calibrated by the incremental addition of a $NaClO_4$ solution ($c$ = 9.94 × 10$^{-3}$ mol dm$^{-3}$) to a 30.0 cm$^3$ solution of


dx.doi.org/10.1021/ic300474s | Inorg. Chem. XXXX, XXX, XXX−XXX

Table 1. Crystallographic Data and Details of Data Collection for the Crystal Structures of L, L·2MeOH, LMeCN, [NaL]$ClO_4$, and [NaLMeCN]barb

| | L | L·2MeOH | LMeCN | [NaL]$ClO_4$ | [NaLMeCN]barb |
|---|---|---|---|---|---|
| molecular formula | $C_{76}H_{116}N_4O_8$ | $C_{78}H_{124}N_4O_{10}$ | $C_{78}H_{121}N_5O_9$ | $C_{76}H_{116}N_4O_{12}NaCl$ | $C_{88}H_{142}N_7O_{15}Na$ |
| $M_r$ | 1213.73 | 1277.81 | 1272.8 | 1336.17 | 1561.09 |
| cryst syst | monoclinic | triclinic | triclinic | tetragonal | triclinic |
| space group | $C2/c$ | $P\bar{1}$ | $P\bar{1}$ | $P4/n$ | $P\bar{1}$ |
| $a$/Å | 31.981(2) | 14.9313(6) | 11.6750(16) | 15.1410(19) | 13.1464(4) |
| $b$/Å | 24.792(2) | 16.3464(8) | 18.183(3) | 15.1410(19) | 16.8767(6) |
| $c$/Å | 18.5200(17) | 18.3108(9) | 20.382(3) | 17.627(3) | 22.1602(8) |
| $\alpha$/deg | 90 | 108.310(4) | 65.402(16) | 90 | 98.404(3) |
| $\beta$/deg | 90.575(7) | 104.079(5) | 74.233(13) | 90 | 90.787(3) |
| $\gamma$/deg | 90 | 106.294(4) | 79.578(13) | 90 | 106.426(3) |
| $V$/Å$^3$ | 14683(2) | 3793.6(3) | 3774.8(10) | 4041.0(9) | 4657.5(3) |
| $Z$ | 8 | 2 | 2 | 2 | 2 |
| $\rho_{calc}$/g cm$^{-3}$ | 1.098 | 1.119 | 1.12 | 1.089 | 1.109 |
| $\lambda$(Mo K$_\alpha$)/Å | 0.71073 | 0.71073 | 0.71073 | 0.71073 | 0.71073 |
| $T$/K | 100.0(2) | 120.0(1) | 120.0(1) | 100.0(2) | 120.0(1) |
| cryst dimens/mm$^3$ | 0.31 × 0.24 × 0.09 | 0.56 × 0.47 × 0.33 | 0.29 × 0.17 × 0.12 | 0.54 × 0.50 × 0.11 | 0.36 × 0.12 × 0.11 |
| $\mu$/mm$^{-1}$ | 0.07 | 0.073 | 0.072 | 0.109 | 0.079 |
| $F$(000) | 5312 | 1400 | 1392 | 1472 | 1688 |
| $\theta$ range/deg | 4−25 | 4−25.5 | 4−25 | 3.72−25 | 3.82−25 |
| $hkl$ ranges | −38, 33; −29, 29; −22, 22 | −18, 16; −19, 19; −22, 21 | −13, 13; −21, 13; −24, 24 | −18, 18; −18, 10; −20, 20 | −15, 15; −18, 20; −24, 26 |
| no. of measd reflns | 45804 | 30764 | 18772 | 23626 | 35524 |
| no. of indep reflns | 12065 | 13514 | 11994 | 3548 | 15632 |
| no. of reflns with $I > 4\sigma(I)$ | 3617 | 6804 | 2591 | 1156 | 8850 |
| no. of param | 888 | 868 | 854 | 320 | 1076 |
| $\Delta\rho_{max}$, $\Delta\rho_{min}$/e Å$^{-3}$ | 0.923, −0.565 | 0.886, −0.6887 | 0.384, −0.272 | 0.343, −0.454 | 1.833, −0.865 |
| $R$ [$F^2 > 4\sigma(F^2)$] | 0.1292 | 0.0511 | 0.061 | 0.1551 | 0.1054 |
| $wR$ ($F^2$) | 0.367 | 0.1304 | 0.1411 | 0.4346 | 0.3246 |
| GOF, $S$ | 0.983 | 1.982 | 0.623 | 1.138 | 1.103 |

$Et_4NClO_4$ ($c$ = 0.01 mol dm$^{-3}$) in MeCN. In each calibration experiment, a Nernstian-like behavior was observed, with the slope of the $E$ versus p[Na] plot being about −58 mV. Titration was repeated three times, and the obtained potentiometric data were analyzed with the *HYPERQUAD* program.[12]

**Conductometry.** Conductometric titrations were carried out at 25.0 ± 0.1 °C by means of a Metrohm 712 conductometer. The cell constant (0.892 ± 0.001 cm$^{-1}$) was determined before each experiment using a 0.01 mol dm$^{-3}$ aqueous KCl solution. The alkali-metal salt solution ($V_0$ = 21.0 or 22.0 cm$^3$ and $c_0$ = 9.0 × 10$^{-5}$−1.16 × 10$^{-4}$ mol dm$^{-3}$) was titrated with a ligand solution ($c$ = 6.58 × 10$^{-4}$−8.21 × 10$^{-4}$ mol dm$^{-3}$) in a thermostatted vessel. The measured conductivities were corrected for the conductivity of the solvent. The obtained data were processed by the *OriginPro7.5* program.

**$^1$H NMR Studies.** $^1$H NMR titrations were carried out at 25 °C by means of a Bruker Avance 600 MHz with a solvent signal used as a standard for titrations in $CD_3CN$ or with a tetramethylsilane (TMS) signal as a standard in $CDCl_3$ solutions. In the titrations of **L** with metal cations in MeCN, solutions made of alkali-metal salt ($c$ = 2.87 × 10$^{-4}$−3.92 × 10$^{-4}$ mol dm$^{-3}$) and **L** ($c$ = 5.32 × 10$^{-4}$ mol dm$^{-3}$) were added in a $CD_3CN$ solution of **L** ($c$ = 5.32 × 10$^{-4}$ mol dm$^{-3}$). In the case of the studies of MeCN binding by **L** and Na**L**$^+$ in $CDCl_3$, solutions of **L** ($c$ = 1.70 × 10$^{-3}$ mol dm$^{-3}$) and [Na**L**]$ClO_4$ ($c$ = 1.24 × 10$^{-4}$ mol dm$^{-3}$) were titrated with a MeCN solution ($c$ = 8.43 × 10$^{-3}$ mol dm$^{-3}$). The temperature dependence of the $^1$H NMR spectrum of **L** was measured in $CD_3CN$ (from −35 to +60 °C) and in $CDCl_3$ (from −50 to +50 °C). Spectra were recorded at 32 pulses.

**Calorimetry.** Microcalorimetric measurements were performed by a Microcal VP-ITC isothermal titration calorimeter at 25.0 °C. The calorimeter was calibrated electrically, and its reliability was additionally checked by carrying out the complexation of $Ba^{2+}$ by 18-crown-6 in a aqueous medium at 25 °C. The results obtained (log $K$ = 3.76 and $\Delta_rH$ = −31.9 kJ mol$^{-1}$) were in good agreement with the literature values (log $K$ = 3.77 and $\Delta_rH$ = −31.4 kJ mol$^{-1}$).[13] Thermograms were processed using the Microcal *OriginPro7.0* program.

In the calorimetric titrations, the enthalpy changes were recorded upon the stepwise additions of a MeCN solution of alkali-metal salt to a solution of **L** ($V_0$ = 1.4182 cm$^3$). Heats of dilution of salt solutions were obtained by blank experiments and subtracted from the heats measured in the titration experiment. The dependence of successive enthalpy changes on the titration volumes was processed by a nonlinear least-squares fitting procedure using the *OriginPro7.5* program. All measurements were conducted three or more times.

**X-ray Structure Determination.** The single crystals of **L**·2MeOH, **L**MeCN, and [Na**L** MeCN]barb (barb = 5,5-diethylbarbiturate) were obtained by the evaporation of a saturated solution at room temperature, while [Na**L**]$ClO_4$ was crystallized by the vapor diffusion of tetrahydrofuran (THF). **L** crystallized from an ethanol solution, **L**·2MeOH from a MeOH solution, and **L**MeCN from a mixture of MeCN, MeOH, and water (5:5:1 volume ratio). Single crystals of [Na**L**MeCN]barb were obtained by the evaporation of a solution prepared by mixing of a solution of sodium 5,5-diethylbarbiturate in a mixture of water and MeOH (1:3) with a MeCN solution of **L**, so that the **L**/$NaC_7H_{11}O_3N_2$ mole ratio was about 1:3.

The crystal and molecular structures were determined by single-crystal X-ray diffraction. Diffraction measurements were made on an Oxford Diffraction Xcalibur Kappa CCD X-ray diffractometer with graphite-monochromated Mo $K_\alpha$ ($\lambda$ = 0.71073 Å) radiation.[14] The data sets were collected using the $\omega$-scan mode over a 2$\theta$ range up to 54°. The structures were solved by direct methods and refined using the *SHELXS* and *SHELXL* programs.[15] The structural refinement was performed on $F^2$ using all data. The hydrogen atoms were placed in calculated positions and treated as riding on their parent atoms [C−H


dx.doi.org/10.1021/ic300474s | Inorg. Chem. XXXX, XXX, XXX−XXX

= 0.93 Å and $U_{iso}(H) = 1.2U_{eq}(C)$; C−H = 0.97 Å and $U_{iso}(H) = 1.2\ U_{eq}(C)$], except those involved in hydrogen bonding, which were located from the electron difference map, if it was possible (in structures of **L**·2MeOH and **L**MeCN). All calculations were performed, and the drawings were prepared using the *WinGX* crystallographic suite of programs.[16] The crystal data and measurement details are listed in Table 1. Further details are available in the Supporting Information and from the Cambridge Crystallographic Centre[17] with quotation numbers 815093−815097.

A number of difficulties were encountered in the refinement of the structural models, mostly because of weak diffraction of the samples and because of the structural disorder of *tert*-butyl and hexyl groups. It was therefore necessary to introduce multiple restraints of bond distances and angles as well as thermal parameters in these parts of the structures. In the structure of **L**, two hexyl chains were modeled as disordered over two positions, although the actual disorder is probably more complex and irresolvable, with hydrophobic parts of the crystal structure resembling a *hydrocarbon glass*. In the structure of **L**·2MeOH, one of the MeOH molecules is disordered and had to be modeled, with the position of the hydroxyl hydrogen atom concluded based on the proximity of an appropriate hydrogen-bond acceptor. The crystal of **L**MeCN was very poorly diffracting, and therefore a large portion of reflections were treated as unobserved, especially at $2\theta$ values above 30°, which has naturally led to problems with resolution and the need for numerous geometrical restraints in the model. In the structure of [Na**L**MeCN]barb, together with a rotational disorder of *tert*-butyl groups, there is an only partly resolvable disorder of the hexyl chains present, similar to, although not as severe as in, **L**. The structure also contains an extensive hydrogen-bonding network with four water molecules independent of symmetry on which the hydrogen atoms could not be located from the electron density map. The most problematic is the structure of [Na**L**]$ClO_4$, where the hexyl chains do not obey the tetragonal crystallographic symmetry of the calixarene *cone* and, therefore, could not be located from the electron density map and had to be modeled. They were modeled as disordered over two sets of positions in order to better account for the residual electron density, which is almost uniform in the entire region occupied by the hexyl groups. In addition, the *tert*-butyl groups and the perchlorate anions are also disordered over two positions. A positional disorder of the perchlorate anions occurred because of placement of both the cations and anions on special positions because the positions are of different multiplicities, with the cations repeated twice and the anions apparently four times within the unit cell. This required the occupancy of the anion to be $^1/_2$ at each site, in order to retain the electric neutrality of the model. It is possible that the latter problem might be resolved by solving and refining the structure in an *I*-centered supercell of quadruple volume. Unfortunately, an attempt of refinement of such a model yielded most unsatisfactory results, with unreasonable bond lengths and *R* of over 35%. However, as has been shown recently,[18] this is not necessarily an indication that the supercell model is incorrect but rather that the diffraction data are not of sufficient quality to support a model with a larger number of refinable parameters. Therefore, it was concluded that the model with the smaller unit cell should be used, even though it may actually represent an average structure.

**DFT Calculations.** Quantum-chemical calculations were performed using the *Gaussian 03* program package[19] with default convergence criteria at the B3LYP/6-311++G(d,p) level of theory. To reduce the computational time and numerical problems, methyl groups were introduced in the substituents at the lower rim (**L′**, Figure 12) instead of the hexyl groups. Geometry optimizations were performed separately for the square *cone* and flattened *cone* conformations of calix[4]arene, and its complex with the $Na^+$ cation placed in the lower-rim hydrophilic cavity. Solvent effects (chloroform and MeCN) were introduced in the calculation using the reformulation of the polarizable continuum method (PCM)[20] known as the integral equation formalism of the PCM of Tomasi and co-workers.[21] In addition, the adduct of **L′** with one MeCN molecule in the hydrophobic *cone* was formed and optimized.

Isotropic shieldings of **L′** and tetramethysilane (TMS) in vacuo and in solvent were calculated by applying the gauge-independent atomic orbital (GIAO) and PCM GIAO[22] methods on the previously optimized geometries using the same basis set as that above. Chemical shifts ($^1$H and $^{13}$C) were calculated with respect to TMS.

**MD Simulations.** The MD simulations were carried out by means of the *GROMACS*[23] package (version 4.5.3). Intramolecular and nonbonded intermolecular interactions were modeled by the OPLS-AA (Optimized Parameters for Liquid Simulations-All Atoms) force field,[24] which has already been successfully used to simulate calix[4]arene derivatives and their complexes with metal cations and/or MeCN.[25] Partial charges assigned to ring carbon atoms bound to $CH_2$ groups that link the monomers were assumed to be zero, as described in ref 25. In all simulations, the initial molecular structure of **L** was the one obtained from the Na**L**$^+$ crystal. The **L** and M**L**$^+$ species were solvated in a cubical box (edge length 58.5 Å) of MeCN with 2156 molecules and with periodic boundary conditions. The solute concentration in such a box was about 0.01 mol dm$^{-3}$. The solvent box was equilibrated prior to inclusion of **L** and its complexes, with the box density after equilibration being close to the experimental one within 5%. During simulations of the systems comprising calixarene and metal cations, the $Cl^-$ ion was included to neutralize the box. The chloride counterion was kept fixed at the box periphery, whereas the complex was initially positioned at the box center. In all simulations, an energy minimization procedure was performed followed by a MD simulation in *NpT* conditions for 50.5 ns, where first 0.2 ns were not used in the data analysis. The Verlet algorithm[26] with a time step of 1 fs was employed.

The cutoff radius for nonbonded van der Waals and short-range Coulomb interactions was 16 Å. Long-range Coulomb interactions were treated by the Ewald method, as implemented in the Particle Mesh Ewald procedure.[27] The simulation temperature was kept at 298.15 K with the Nosé−Hoover[28] algorithm using a time constant of 1 ps. The pressure was kept at 1 bar by the Martyna−Tuckerman−Tobias−Klein[29] algorithm and a time constant of 1 ps.

## RESULTS AND DISCUSSION

**Synthesis.** Calix[4]arene tetrahexylamide **L** was synthesized according to the previously described method,[5b] starting from the corresponding tetraester (*cone* conformation) by (i) hydrolysis to the tetraacid, (ii) activation to the acid chloride,[10] and (iii) amide bond formation (Scheme 1). Alternatively, the same compound can be prepared via aminolysis of the tetraester with *n*-hexylamine, as described in the Experimental Section.

**Crystal Structures and Stereochemistries of L, L·2MeOH, LMeCN, [NaL]$ClO_4$, and [NaLMeCN]barb.** Solvent-free crystals of **L** were obtained from its ethanol (EtOH) solution, while crystallization from MeOH yielded a MeOH solvate, **L**·2MeOH, with two MeOH molecules per molecule of **L**.

In the solvent-free crystal and the MeOH solvate, the molecular structure of **L** (Figure 1) revealed almost identical distorted calixarene *cones* of an approximate $C_2$ symmetry (Figure 2). The *cone* is characterized by alternating signs of the torsion angles $\varphi$ and $\chi$ (Table S1, Supporting Information) about the methylene bonds of the macrocyclic ring.[30] Deformation of the *cone* can be described as tilting of the phenyl rings toward the macrocycle plane defined by the methylene carbon atoms. In the molecule of **L**, two rings are almost parallel (the planes of the rings are at an angle of 1.6° in **L** and 2.7° in **L**·2MeOH) and almost perpendicular to the plane of the macrocycle (81.6° and 80.7° in **L**; 82.0° and 84.6° in **L**·2MeOH). The other two rings are tilted from the macrocycle plane with angles of the phenyl rings to the plane of 42.0° and 48.3° in **L** (44.5° and 40.3° in **L**·2MeOH). The


dx.doi.org/10.1021/ic300474s | Inorg. Chem. XXXX, XXX, XXX−XXX

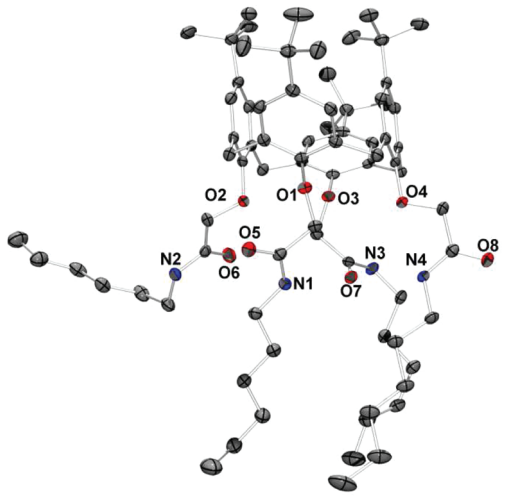


**Figure 1.** ORTEP plot of the **L** molecule in the structure of **L**·2MeOH with the labeling scheme for non-carbon atoms. Thermal ellipsoids are shown with 50% probability. Hydrogen atoms as well as minor components of all disordered groups have been omitted for clarity. The labeling of the atoms is analogous in all of the structures.

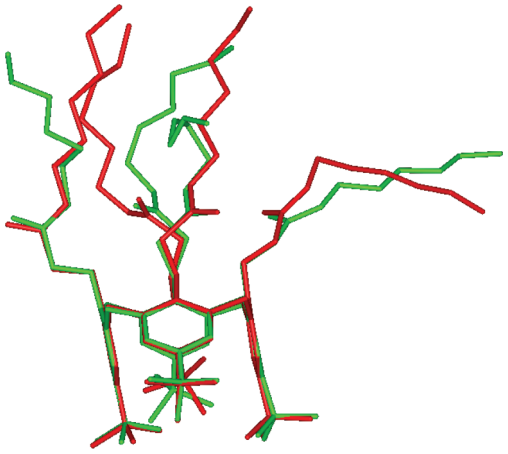

**Figure 2.** Overlap of the molecules of **L** from the crystal structures of the solvent-free crystal (green) and the MeOH solvate (red), showing almost identical *cone* geometry in the two crystals. Hydrogen atoms as well as minor components of all disordered groups have been omitted for clarity.

planes of the latter two rings are almost perpendicular to each other, being at an angle of 89.7° (84.6° in **L**·2MeOH).

In the crystal structure of the solvent-free **L**, there is an extensive network of hydrogen bonds present. Two amide nitrogen atoms participate in an intramolecular hydrogen bond with the same carbonyl oxygen atom (N2−H2n···O8 and N3−H3n···O8), while the other nitrogen atoms are hydrogen-bonded to carbonyl groups of neighboring molecules (N1−H1n···O6 and N4−H4n···O7), forming a 2D hydrogen-bonding network parallel to the *bc* plane (Table S2, Supporting Information). Out of four carbonyl oxygen atoms, only O5 does not participate in strong hydrogen bonding but is in close contact with hydrogen atoms from two methylene groups, namely, C68−H68a from the same molecule and C60−H60a from the neighboring one.

The intramolecular hydrogen bonding in the crystal structure of the MeOH solvate (**L**·2MeOH) is very similar to that in solvent-free **L** (Figure 3a,b) because here also two amide

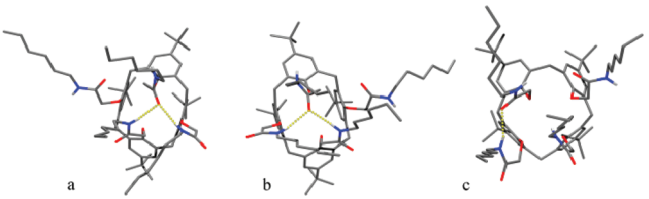


**Figure 3.** Intramolecular hydrogen bonding in crystal structures of (a) a solvent-free crystal of **L**, (b) the MeOH solvate **L**·2MeOH, and (c) the **L**MeCN adduct. Hydrogen atoms bonded to carbon atoms of **L** and solvent molecules have been omitted for clarity.

nitrogen atoms are hydrogen-bonded to one carboxyl oxygen atom, forming two intramolecular hydrogen bonds (N1−H1···O7 and N4−H4···O7). The remaining amide groups participate in intermolecular hydrogen bonding, either with neighboring molecules of **L** (two bonds N2−H2···O5) or with MeOH molecules of which one acts only as hydrogen donor to an amide oxygen atom (O10−H···O6), while the other is bridging between two molecules of **L** (O9−H···O8 and N3−H···O9). The hydrogen-bonding network interconnects the molecules in chains along the [101] direction (Table S2, Supporting Information).

Crystallization of **L** from a mixture of MeCN, MeOH, and water yielded **L**MeCN monohydrate. The MeCN molecule is situated in the calixarene *cone*, with the methyl group of the MeCN forming a weak C−H···$\pi$ hydrogen bond with the aromatic rings of the *cone* (C···centroid distances between 3.413 and 3.783 Å; Figure 4a). The *cone* is much more regular

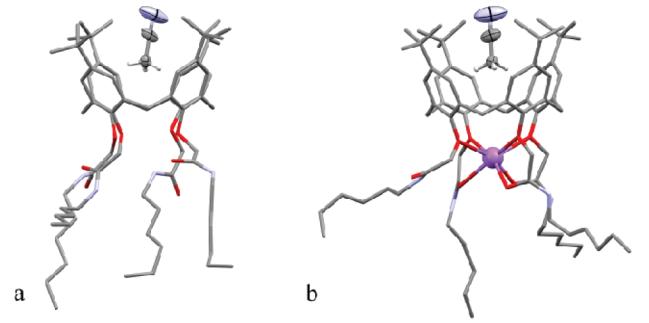


**Figure 4.** Position of the MeCN molecule nested in the calixarene *cone* in crystal structures of (a) **L**MeCN and (b) [Na**L**MeCN]barb. The non-hydrogen atoms of the MeCN molecules are shown as thermal motion ellipsoids plotted with 50% probability, and the MeCN hydrogen atoms are shown as small spheres of arbitrary radius. The hydrogen atoms of the calixarene unit have been omitted for clarity.

than when MeCN is absent, although it is still somewhat flattened (Figure 5). The angles of phenyl rings to the macrocycle plane are 74.74°, 68.27°, 58.00°, and 57.58°. Of the four N−H groups, one is involved in an intramolecular hydrogen bond (N3−H3···O6; Figure 3c) and one (N4−H4) is positioned so that the hydrogen atom is positioned toward the calixarene macrocycle and approximately equidistant (ca 2.73 Å) to ether oxygen atoms (O1, O2, and O3). N2−H2 forms a hydrogen bond with a water molecule, which further bonds via O9−H6···O5 to a carbonyl oxygen atom of the same calixarene molecule and via O9−H5···O7 to a carbonyl oxygen atom of a neighboring calixarene molecule. The remaining N1−H1 bonds via N1−H1···O8 to a neighboring calixarene molecule (Table S2, Supporting Information). The intermo-


dx.doi.org/10.1021/ic300474s | *Inorg. Chem.* XXXX, XXX, XXX−XXX

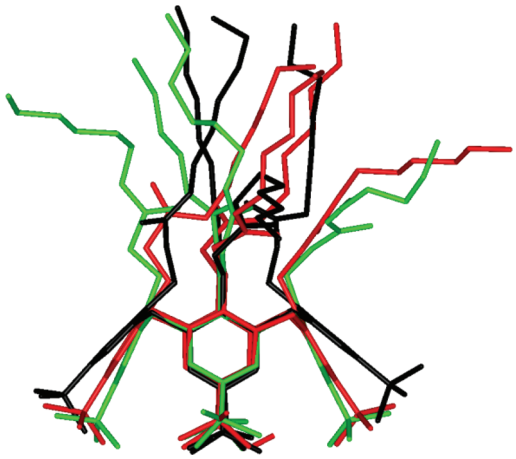

**Figure 5.** Overlap of the molecules of **L** from the crystal structures of **L**·2MeOH, (black), the MeCN adduct **L**MeCN (red), and the sodium complex [Na**L**]$ClO_4$ (green). Hydrogen atoms have been omitted for clarity.

lecular hydrogen bonding forms a double chain of molecules along the [100] direction.

In [Na**L**]$ClO_4$, the sodium ion is located on the crystallographic 4-fold axis. The coordination polyhedron around the sodium atom is an intermediate between a cube and a square antiprism and is formed by four ether and four carbonyl oxygen atoms with Na−O bond lengths of 2.556(5) and 2.368(17) Å, respectively. The *cone* is of perfectly regular conformation of $C_4$ symmetry (positioned on a crystallographic 4-fold axis; Figure 5). Phenyl rings are at an angle of 67.29° to the macrocycle plane. Amide nitrogen atoms from $[NaL]^+$ moieties form hydrogen bonds with perchlorate ions, which, in turn, bridge to further $[NaL]^+$ ions, thus forming a 2D network perpendicular to the [100] direction.

Unfortunately, the hexyl groups disobeyed the $C_4$ crystallographic symmetry, causing severe and irresolvable disorder. In addition, the *tert*-butyl groups, the perchlorate anion, and the solvent water present in the structure are also in disorder, reducing the quality of the structural model. To overcome this problem, a second complex was prepared, using sodium 5,5-diethylbarbiturate instead of perchlorate. It was presumed that such a complex will not crystallize in the tetragonal system, thus allowing the ordering of the hexyl groups. The crystallization of this complex from a mixture of MeCN, MeOH, and water yielded [Na**L**MeCN]barb MeOH monosolvate tetrahydrate. With the expected lowering of the symmetry, an unexpected change in the geometry of $[NaL]^+$ also occurred. The coordination number of the sodium atom was no longer 8 but 7, with one of the amide groups rotated by approximately 180°, so that instead of carbonyl oxygen bonding to the central sodium, the amide nitrogen forms a hydrogen bond (N1−H1···O6) with a coordinated carbonyl oxygen. The coordination polyhedron of the sodium atom can be described as a square-face monocapped trigonal prism. The calixarene *cone* is of regular conformation (approximate $C_4$ symmetry), and the values of the angles between the phenyl rings and the macrocycle plane of 64.47°, 64.67°, 66.32°, and 66.67° approach the value of 67.29° found in the structure of [Na**L**]$ClO_4$ (Figure 6). Like in the structure of **L**MeCN, the MeCN molecule is situated in the calixarene *cone*, with the methyl group of the MeCN forming a weak C−H···$\pi$ hydrogen bond with the aromatic rings of the *cone* (C···centroid distances

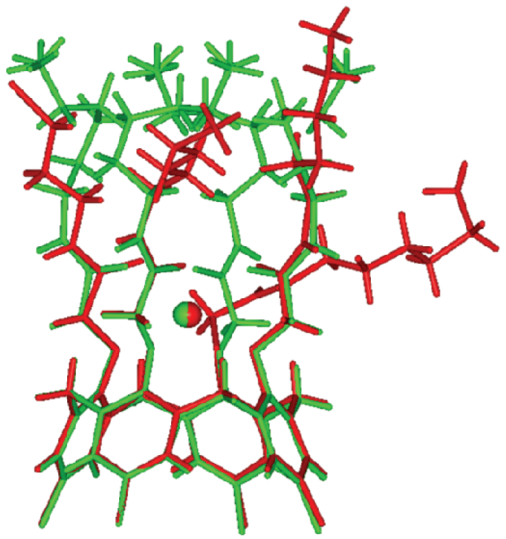

**Figure 6.** Overlap of the $[NaL]^+$ ions from the crystal structures of [Na**L**]$ClO_4$ (green) and [Na**L**MeCN]barb (red). *tert*-Butyl groups have been omitted for clarity.

between 3.563 and 3.610 Å; Figure 4b). In addition to the intermolecular hydrogen bond mentioned above, the $[NaL]^+$ ion participates in an extensive hydrogen-bonding network, which also includes the 5,5-diethylbarbiturate anion, ethanol, and four symmetrically independent water molecules. This intermolecular hydrogen bonding forms a double chain of molecules along the [100] direction.

**Structural Studies of L in Solution.** The structure of the investigated calix[4]arene derivative in solution was studied by means of $^1$H NMR spectroscopy. Three solvents were used, namely, deuterated chloroform, methanol, and acetonitrile. The $^1$H NMR spectrum of **L** in $CDCl_3$ (Figure S6 and Table S3, Supporting Information) showed two singlets at 1.08 and 6.77 ppm due to *tert*-butyl groups and calixarene aromatic protons (Ar−H), respectively. In addition, two sets of doublets due to the bridging methylene protons (3.23 and 4.47 ppm) were observed along with the singlet at 4.75 ppm, which corresponds to $ArOCH_2$ protons. Such a pattern is characteristic for the *cone* conformation with $C_{4v}$ symmetry or time-averaged $C_{4v}$ conformation of tetrasubstituted calix[4]arenes.[1e] A rather high chemical shift of NH protons (7.46 ppm) indicated the presence of intramolecular NH···O=C hydrogen bonds.[5a,b] The spectrum of **L** in $CD_3OD$ (Figure S6 and Table S3, Supporting Information) was basically similar (apart from the absence of the NH signal). On the other hand, the $^1$H NMR spectrum of **L** in $CD_3CN$ was quite different, being characterized by two sets of signals, i.e., two signals for each of the ligand protons with unequal integrals (Figure 7 and Table S3, Supporting Information). This interesting finding can be explained by taking into account the possibility of inclusion of a MeCN molecule into the calixarene hydrophobic cavity, which is well documented in the literature[4a−f,5k,7] and observed in the crystal structure of **L**MeCN. Thus, the presence of two sets of signals indicates the existence of an equilibrium between the "free" ligand and the one with a bound MeCN molecule. For example, two singlets assigned to ArH protons appeared at 7.33 ppm (3.24 H) and 7.12 ppm (4.76 H). Because the downfield shift of the ArH signal can be taken as an indication of the interaction of the MeCN molecule with the calix[4]arene aromatic rings,[7a,8a] the lower field resonance can be attributed


dx.doi.org/10.1021/ic300474s | *Inorg. Chem.* XXXX, XXX, XXX−XXX

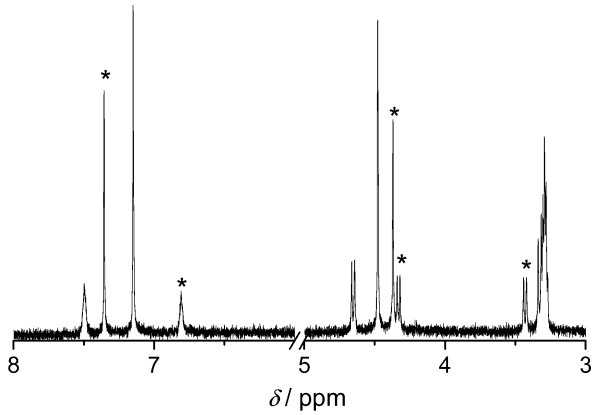


**Figure 7.** $^1$H NMR spectrum of **L** in $CD_3CN$. Signals corresponding to the **L**MeCN species are labeled by asterisks.

to the **L**MeCN species and the higher field one to the free ligand. The complete assignment of the signals in the $^1$H NMR spectrum of **L** in $CD_3CN$ was carried out with the aid of the results of computational studies, temperature dependence of the **L** NMR spectrum, and NMR titrations of **L** with metal salt solutions (see below).

The equilibrium constant for the reaction of inclusion of the MeCN molecule in the **L** hydrophobic cavity (**L** + MeCN ⇄ **L**MeCN) can be calculated as a ratio of integrals of signals corresponding to **L** and **L**MeCN. At 25 °C, it amounts to 0.68 (estimated from the integrals of signals corresponding to ArH and *tert*-butyl protons).

Temperature dependences of $^1$H NMR spectra of **L** in $CDCl_3$ and $CD_3CN$ are shown in Figures S7 and S8 (Supporting Information). Upon heating from −50 to +50 °C, the only considerable change observed in chloroform was that of the chemical shift of the amide NH protons, which was shifted upfield. That was expected as a consequence of intramolecular NH···O═C hydrogen-bond cleavage.[5b] The situation was much more interesting in the case of MeCN. The intensities of the signals belonging to the one set of **L** signals (denoted by asterisks in Figure 7) gradually decreased with an increase in the temperature, whereas those of the other set increased. Because inclusion of the MeCN molecule in the hydrophobic cavity of calix[4]arene is known to be exothermic,[4c,d] the observed changes can be explained by taking into account that with increasing temperature the equilibrium between **L** and **L**MeCN species is shifted toward the free ligand. This finding can serve as an additional corroboration of the assignment of the ligand $^1$H NMR signals presented in Figure 7.

**Studies of Cation Complexation in Solution.** Stability constants of the Li**L**$^+$, Na**L**$^+$, and K**L**$^+$ complexes in MeCN were determined by microcalorimetric, spectrophotometric (K**L**$^+$), conductometric (K**L**$^+$), and potentiometric (Na**L**$^+$) titrations, and the obtained values are given in Table 2.

The UV spectral changes observed upon the addition of $LiClO_4$, $NaClO_4$, or $KClO_4$ to the solution of **L** in MeCN were qualitatively similar. In all cases, the ligand UV spectrum exhibited a hypochromic shift of its larger part, accompanied by the occurrence of a well-defined isosbestic point. The spectrophotometric titration of **L** with $K^+$ is shown in Figure 8, and the stability constant of the K**L**$^+$ complex computed by processing these data is given in Table 2. The stability constants of the Li**L**$^+$ and Na**L**$^+$ complexes were too large to be determined spectrometrically because of the limited sensitivity of this method. However, the strong complexation and 1:1

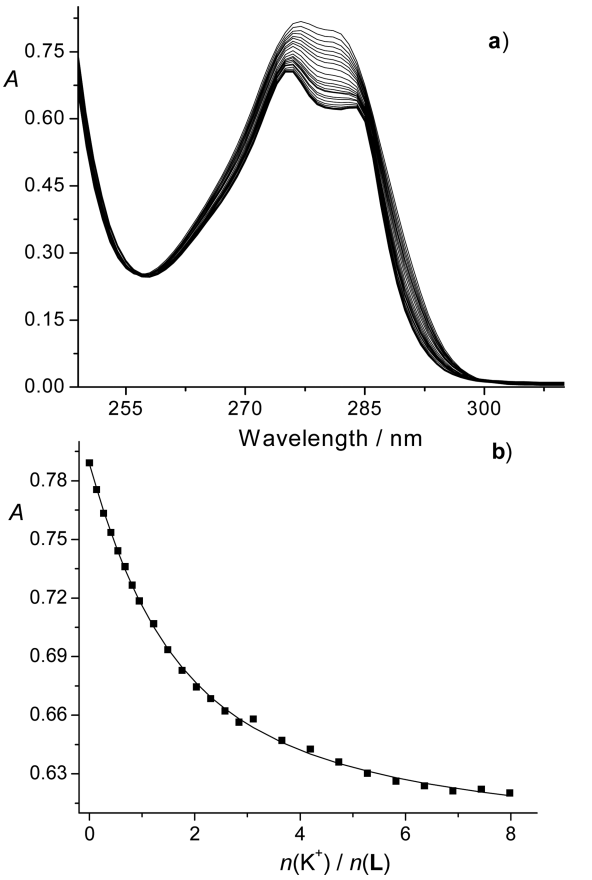


**Figure 8.** (a) Spectrophotometric titration of **L** ($c = 2.57 \times 10^{-4}$ mol dm$^{-3}$ and $V_0 = 2.0$ cm$^3$) with $KClO_4$ ($c = 3.3 \times 10^{-3}$ mol dm$^{-3}$) in MeCN. $I_c = 0.1$ mol dm$^{-3}$ ($Et_4NClO_4$); $t = 25.0 \pm 0.1$ °C. Spectra are corrected for dilution. (b) Dependence of the absorbance at 282 nm on the $n(K^+)/n(L)$ ratio: (■) experimental; (—) calculated.

**Table 2. Stability Constants of Complexes of Alkali-Metal Cations with L in MeCN at 25 °C**

| | log $K \pm$ SE | | | |
|---|---|---|---|---|
| cation | calorimetry | spectrophotometry | conductometry | potentiometry |
| $Li^+$ | 6.04 ± 0.05 | >5 | >5 | |
| $Na^+$ | 6.88 ± 0.05 | >5 | >5 | 6.93 ± 0.03 |
| $K^+$ | 3.61 ± 0.02 | 3.54 ± 0.02 | 3.56 | |
| $Rb^+$ | *a* | *a* | *a* | |
| $Cs^+$ | *a* | *a* | *a* | |

[a]No complexation was observed. SE = standard error of the mean ($N$ = 3–4).


dx.doi.org/10.1021/ic300474s | *Inorg. Chem.* XXXX, XXX, XXX–XXX

($M^+$/**L**) stoichiometry of these complexes were undoubtly proven by the almost linear dependence of the absorbance on the $n(M^+)/n(\mathbf{L})$ ratio ($n$ denotes the total amount), followed by a break in the titration curve at a molar ratio of approximately 1 (Figure S14, Supporting Information). The addition of $Rb^+$ and $Cs^+$ nitrates in the MeCN solution of **L** did not cause any significant changes in its UV spectrum, indicating that complexation of larger cations by the ligand was very weak or nonexistent.

The above results were confirmed by conductometric measurements. In the cases of $LiClO_4$, $NaClO_4$, and $KClO_4$ solutions, the conductivity (corrected for dilution) decreased upon the addition of the ligand (due to a lower electric mobility of the larger $ML^+$ complex compared to that of the free cation), whereas during titrations of $RbNO_3$ and $CsNO_3$ solutions with **L**, almost no change of the conductivity was observed. As can be seen in Figure S15 (Supporting Information), in the titrations of $LiClO_4$ and $NaClO_4$ solutions, the conductivity decreased almost linearly with the amount of ligand added, and at the molar ratio $n(\mathbf{L})/n(M^+) \approx 1$, a break in the titration curve occurred. On the other hand, in the case of $KClO_4$, the $\kappa$ versus $n(\mathbf{L})$ dependence was curved (Figure 9), which allowed

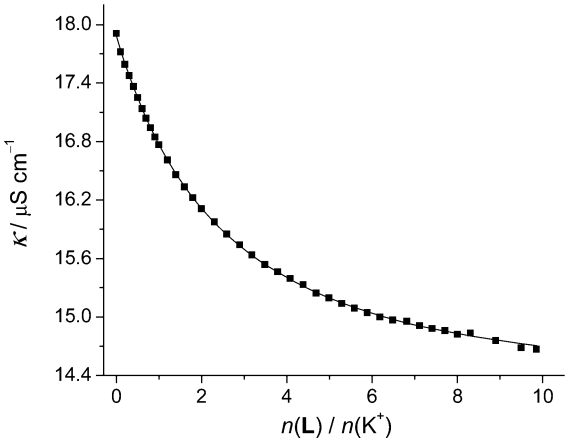


**Figure 9.** Conductometric titration of $KClO_4$ ($c = 9.7 \times 10^{-5}$ mol dm$^{-3}$ and $V_0 = 21.0$ cm$^3$) with **L** ($c = 6.51 \times 10^{-4}$ mol dm$^{-3}$ and $7.26 \times 10^{-4}$ mol dm$^{-3}$) in MeCN: (■) experimental; (—) calculated. $t = 25.0 \pm 0.1$ °C. Conductivities are corrected for dilution.

for calculation of the $KL^+$ stability constant by nonlinear regression analysis of the titration data (nonspecific, i.e., electrostatic, interactions affecting the conductivity were not taken into account). The obtained value was in excellent agreement with those determined by microcalorimetric and spectrophotometric measurements (Table 2). It should be noted that the assessed molar conductivities of the $[LiL]ClO_4$ (136 S cm$^2$ mol$^{-1}$), $[NaL]ClO_4$ (136 S cm$^2$ mol$^{-1}$), and $[KL]ClO_4$ (129 S cm$^2$ mol$^{-1}$) species were similar. That could be expected if one neglects the ionic interactions and by taking into account that the size of the conducting complex is mainly determined by the size of the ligand involved.[5i]

The stability constant of the $NaL^+$ complex was determined by direct potentiometry using a sodium-selective glass electrode. The corresponding titration curve exhibited an inflection point at $n(\mathbf{L})/n(Na^+) \approx 1$ (Figure 10). The equilibrium constant for the complexation reaction between $Na^+$ and **L** obtained by processing the potentiometric data was

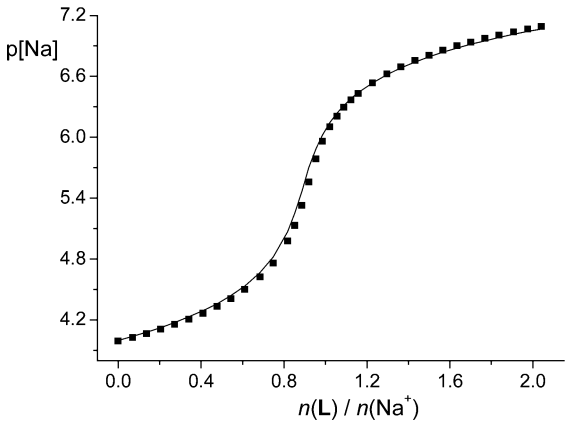


**Figure 10.** Potentiometric titration of $NaClO_4$ ($c = 1 \times 10^{-4}$ mol dm$^{-3}$ and $V_0 = 30.24$ cm$^3$) with **L** ($c = 7.68 \times 10^{-4}$ mol dm$^{-3}$) in MeCN: (■) experimental; (—) calculated. $I_c = 0.01$ mol dm$^{-3}$ ($Et_4NClO_4$); $t = 25.0 \pm 0.1$ °C.

quite high (Table 2), in agreement with the results of the other measurements conducted in this work.

The thermodynamic parameters obtained by microcalorimetric titrations are summarized in Table 3. The stepwise

**Table 3. Thermodynamic Parameters for Complexation of Alkali-Metal Cations with L in MeCN at 25 °C Obtained by Calorimetry[a]**

| cation | $(\Delta_rG^\circ \pm SE)$/kJ mol$^{-1}$ | $(\Delta_rH^\circ \pm SE)$/kJ mol$^{-1}$ | $(\Delta_rS^\circ \pm SE)$/J K$^{-1}$ mol$^{-1}$ |
|---|---|---|---|
| $Li^+$ | −34.5 ± 0.2 | −12.9 ± 0.1 | 72.3 ± 0.8 |
| $Na^+$ | −39.3 ± 0.1 | −33.8 ± 0.2 | 18.5 ± 1.2 |
| $K^+$ | −20.63 ± 0.04 | −19.7 ± 0.4 | 3.1 ± 1.3 |

[a]SE = standard error of the mean ($N = 3$–5).

addition of a $LiClO_4$, $NaClO_4$, or $KClO_4$ solution to the MeCN solution of **L** resulted in exothermic enthalpy changes. Standard reaction enthalpies and equilibrium constants were computed by least-squares nonlinear analysis of the calorimetric data. As an example, the experimental and fitted data corresponding to the titration of **L** with $Na^+$ are shown in Figure 11 (the results of other calorimetric measurements are given in Figures S14 and S15, Supporting Information). Standard reaction Gibbs energies and entropies were obtained by means of the well-known equations $\Delta_rG^\circ = -RT \ln K$ and $\Delta_rG^\circ = \Delta_rH^\circ - T\Delta_rS^\circ$, respectively.

The stability constant of the $NaL^+$ complex might seem to be too large to be determined accurately from a microcalorimetric direct titration experiment. However, its value obtained in that way is in very good agreement with the one measured by potentiometric titrations (Table 2). In addition, it should be noted that the validity of our experimental and fitting procedure was also checked by performing the simulations suggested by Bäckman et al.[31]

The addition of $RbNO_3$ or $CsNO_3$ to the investigated calixarene solution did not cause any significant heat effects. These findings suggested that no complexation took place under the conditions used or that the values of the corresponding reaction enthalpies were close to zero. However, by taking into account the spectrophotometric and conductometric findings, it can be concluded that the investigated calix[4]arene ion-binding site was not suitable for $Rb^+$ and $Cs^+$ cations.


dx.doi.org/10.1021/ic300474s | Inorg. Chem. XXXX, XXX, XXX–XXX

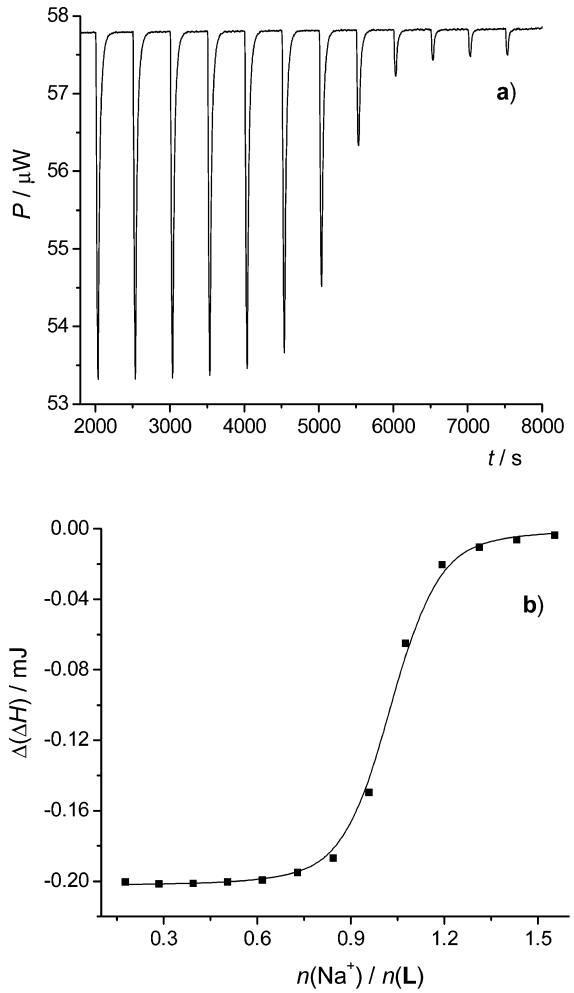


**Figure 11.** (a) Microcalorimetric titration of **L** ($c$ = 4.0 × $10^{-5}$ mol $dm^{-3}$ and $V$ = 1.4182 $cm^3$) with $NaClO_4$ ($c$ = 4.0 × $10^{-4}$ mol $dm^{-3}$) in MeCN: $t$ = 25 °C. (b) Dependence of successive enthalpy changes on the $n(Na^+)/n(\mathbf{L})$ ratio. (■) experimental; (—) calculated.

The data presented in Table 3 indicate that both enthalpic and entropic contributions to the reaction Gibbs energy for complexation of $Li^+$, $Na^+$, and $K^+$ are favorable. However, the mutual relations of these contributions are substantially different. The complexation entropy is most favorable for $Li^+$ binding with **L**, whereas the $-\Delta_r H°$ value is the lowest for this reaction. As described elsewhere,[5k] this could be partly explained by a stronger solvation of the $Li^+$ cation compared to the other alkali-metal ions. The enthalpic and overall thermodynamic stability is the largest in the case of the Na**L**$^+$ complex. The value of the reaction enthalpy for $K^+$ complexation with **L** is between those for $Li^+$ and $Na^+$, whereas the entropic contribution to the binding Gibbs energy is in this case considerably lower (almost negligible at the standard state of 1 mol $dm^{-3}$; Table 3). That is reflected in the lowest stability of the K**L**$^+$ species compared to Na**L**$^+$ and Li**L**$^+$ in MeCN.

In addition to the experiments described above, the reactions of $Li^+$, $Na^+$, and $K^+$ with **L** in MeCN were also followed by $^1$H NMR titrations. The complexation-induced changes of the **L** spectrum were different for each cation studied. In the case of $Na^+$, below a stoichiometric 1:1 ($NaClO_4$/**L**) ratio, two distinct, separate resonances for the Na**L**$^+$ complex and the free ligand were present simultaneously (Figure S9, Supporting Information). Interestingly, the positions of signals belonging to the complexed (e.g., Ar−H, 7.33 ppm) and uncomplexed ligand (Ar−H, 7.12 ppm) were at practically the same chemical shifts as those corresponding to the **L**MeCN and **L** species, respectively. In other words, the positions of these signals remained almost the same during titration, whereby their intensities changed (Figure S9, Supporting Information). Above a molar ratio of approximately 1:1, the spectrum consisted of a single set of signals (chemical shifts being almost equal to those of **L**MeCN) that did not change with an increase in the amount of $NaClO_4$. The findings described strongly suggest that conformations of **L**MeCN and the sodium complex with **L** in MeCN are very similar. Moreover, one can conclude that the $Na^+$−**L** complex species predominantly possesses a MeCN molecule included in its hydrophobic cavity.

To examine in more detail the interactions of the investigated calixarene and its sodium complex with the MeCN molecule, $^1$H NMR titrations of these species with MeCN in deuterated chloroform were carried out. The formation of the **L**MeCN adduct could not be detected because, during titration of **L** with MeCN (Figure S12, Supporting Information), the chemical shift of $CH_3CN$ protons in the MeCN/**L** molar ratio range 3:1 showed no difference with respect to the corresponing signal of MeCN in $CDCl_3$ (2.0 ppm). Likewise, no significant change of the chemical shifts of **L** protons could be observed. That is most likely a consequence of the rather low extent of MeCN inclusion in the **L** hydrophobic cavity under the stoichiometric conditions applied. On the other hand, binding of MeCN with the Na**L**$^+$ complex was clearly indicated. At the lowest MeCN/Na**L**$^+$ molar ratio examined (0.27), the signal of MeCN protons appeared at 1.80 ppm (upfield shift) and then gradually shifted toward the position of the MeCN signal in $CDCl_3$ (Figure S13, Supporting Information). Moreover, the signals of the **L** protons also exhibited shifts with increasing MeCN concentration. It should be noted that in chloroform an extensive ion pairing between Na**L**$^+$ and $ClO_4^-$ ions is likely to occur and that can have an impact on the process of MeCN molecule inclusion. However, the extent of this impact is hard to assess.

The above results show that the affinity of the Na**L**$^+$ complex toward MeCN is much higher than that of the free ligand. The reason lies in the fact that in the case of Na**L**$^+$ the ligand hydrophobic cavity is better preorganized to accept the MeCN molecule.[4f,5k,8c]

Formation of the complex of **L** with $Li^+$ was accompanied by the shifts and broadening of the resonances attributed to **L** (without MeCN) species up to the $n(Li^+)/n(\mathbf{L})$ ratio ≈1, whereas the positions of the signals belonging to **L**MeCN remained practically unchanged (Figure S10, Supporting Information). This indicated that, compared to the reaction of $Na^+$ with **L**, the exchange kinetics of complexation of $Li^+$ by **L** was faster. Beyond the molar ratio of approximately 1, no further spectral changes occurred, and two distinct sets of signals were observed (Figure S10, Supporting Information). The latter was likely to be a consequence of the existence of an equilibrium between two types of Li$^+$**L** complexes, i.e., one with (Li**L**MeCN$^+$) and the other without (Li**L**$^+$) a specifically bound MeCN molecule. The corresponding complexation processes are presented in Scheme 2.

$K_1$ and $K_4$ denote the equilibrium constants of the MeCN binding reactions with the free ligand and Li**L**$^+$ complex, respectively. The value of $K_4$ was assessed to be 0.88 from the ratio of integrals of $^1$H NMR peaks assigned to the Li**L**MeCN$^+$ and Li**L**$^+$ species, whereas $K_1$ = 0.68 was estimated earlier (see


dx.doi.org/10.1021/ic300474s | Inorg. Chem. XXXX, XXX, XXX−XXX

**Scheme 2. Chemical Equilibria Corresponding to the Binding of $Li^+$ Cation by L**

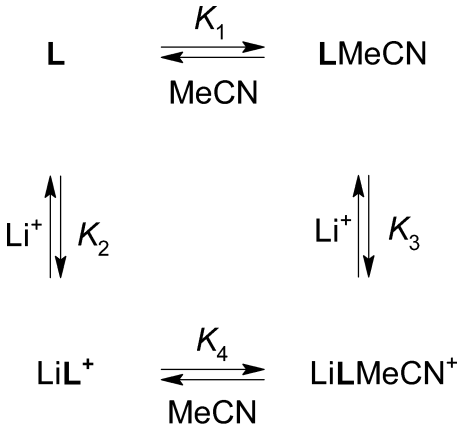


above). It can be easily shown that these constants are related to the microscopic complexation equilibrium constants $K_2$ and $K_3$ in the following way:

$$\frac{K_1}{K_4} = \frac{K_2}{K_3} \tag{2}$$

The macroscopic stability constant $K$ determined calorimetrically (Table 2) can be expressed as

$$K = \frac{[\mathrm{LiL}^+] + [\mathrm{LiLMeCN}^+]}{[\mathrm{Li}^+]\{[\mathbf{L}] + [\mathbf{L}\mathrm{MeCN}]\}} \tag{3}$$

or

$$K = \frac{K_2 + K_1K_3}{1 + K_1} \tag{4}$$

By combining eqs 2 and 4, one can calculate the values of microscopic constants $K_2$ and $K_3$, which were found to be $9.8 \times 10^5$ and $1.3 \times 10^6$, respectively.

Like with lithium, the equilibrium kinetics of the **L** complex with $K^+$ was found to be fast on the NMR time scale. That can be easily concluded by inspecting Figure S11 (Supporting Information), which shows changes of the ligand spectrum occurring during its titration with $KClO_4$ in deuterated MeCN. The peaks corresponding to the macrocycle without MeCN in its hydrophobic cavity exhibited broadening and shifting, while the positions of the **L**MeCN peaks did not change, but their intensities decreased with an increase in the amount of $K^+$ ion. Complete calixarene complexation could not be achieved experimentally because of the insufficiently high stability constant of the $K^+$**L** complex(es) and insufficient solubility of $KClO_4$ in MeCN. However, the $^1H$ NMR spectrum of **L** in the solution saturated with $KClO_4$ (Figure S11, Supporting Information) indicates that most probably the complex species almost exclusively comprises a MeCN molecule in its aromatic *basket*. Like in the case of the complex with $Na^+$, a single peak of ArH protons appeared at 7.33 ppm and the one attributed to the *tert*-butyl protons at 1.21 ppm (chemical shifts that almost completely correspond to those observed for **L**MeCN, Na**L**MeCN$^+$, and Li**L**MeCN$^+$ species).

**Quantum-Chemical Computations.** Geometry optimizations were performed separately for square *cone* and flattened *cone* conformations ($C_4$ and $C_2$ point groups, respectively; Figure 12) of model calix[4]arene molecule **L**′ with hexyl groups replaced by methyl groups.

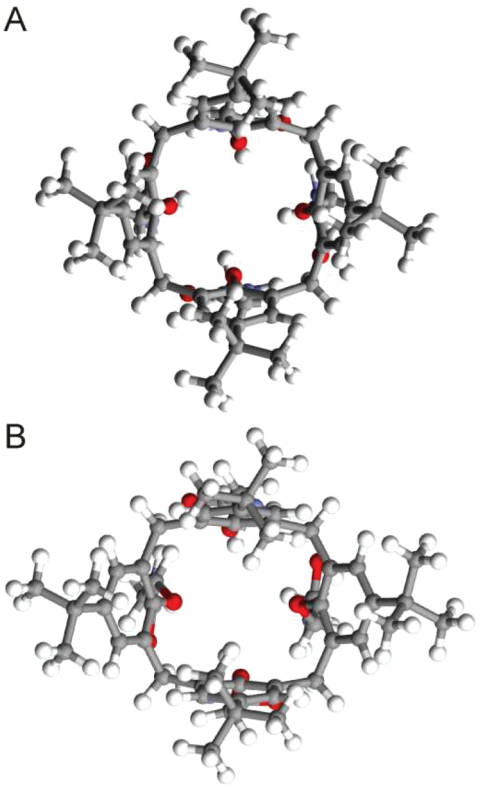


**Figure 12.** Molecular structures of the square *cone* (A; $C_4$ point group) and flattened *cone* (B; $C_2$ point group) conformations of the model calix[4]arene **L**′ optimized at the B3LYP/6-311++G(d,p) level of theory.

The DFT calculations showed that the difference in energy is approximately 4 kJ $mol^{-1}$ in favor of the flattened *cone* conformation. That difference is probably due to the reduced steric repulsion between *tert*-butyl groups in the flattened *cone* conformation. The minimal distance between protons of neighboring *tert*-butyl groups is 2.849 Å for the square *cone* conformation, whereas in the case of the flattened *cone* conformation, these distances are 3.197 and 3.257 Å, thus giving a more relaxed structure. This could also explain why **L** adopts this conformation in the crystal structures of both **L** and its MeOH solvate. In the square *cone* conformation, there are four equivalent hydrogen bonds between each carbonyl oxygen atom and the nitrogen atom with the distance $r_{ON}$ = 2.949 Å and the angle $\alpha_{OHN}$ = 155.5°. In the flattened *cone* conformation, there are two equivalent sets of these hydrogen bonds with the distances and angles of 2.908 Å (148.4°) and 3.086 Å (167.2°).

In order to investigate the effect that binding of the MeCN molecule has on the structure of calix[4]arene, an adduct with a MeCN molecule in the hydrophobic cavity was formed and optimized (Figure 13).

The structure of this species is similar to the square *cone* conformation of free **L**′ (distances between protons of neighboring *tert*-butyl groups are in the range from 2.908 to 3.075 Å, while the hydrogen bonds remain essentially the same). The position of the MeCN molecule inside the *cone* is slightly tilted from the centerline (a similar structure was obtained using the B97D functional). That position indicates a possibility of active movement of the solvent molecule inside the calix[4]arene molecule cavity. This conclusion is also supported by the crystal structure of the MeCN solvate of **L**,


dx.doi.org/10.1021/ic300474s | *Inorg. Chem.* XXXX, XXX, XXX–XXX

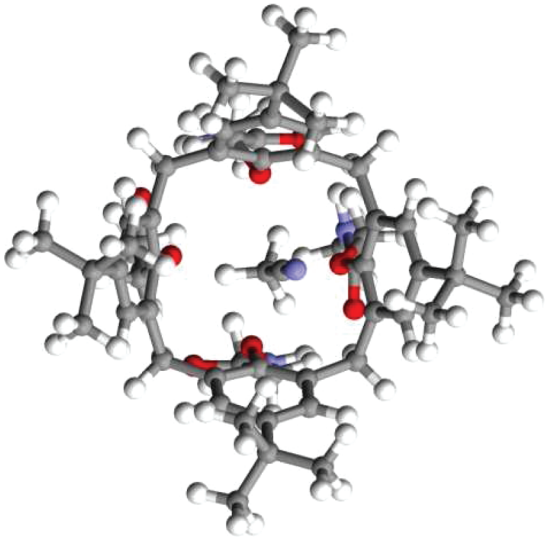

**Figure 13.** Molecular structure of **L**′ with an explicit molecule of MeCN in the hydrophobic cavity optimized at the B3LYP/6-311++G(d,p) level of theory.

where together with the sloping of the MeCN molecule an elongation of the thermal motion ellipsoids of the MeCN cyano group is noticed (Figure 4), which indicates a motion of the molecule with the methyl group fixed in the macrocycle *cone* and the cyano group oscillating perpendicularly to the calixarene molecular axis. Therefore, in order to investigate in more detail the solvent effects on the molecular structure of calix[4]arene, MD simulations have been carried out.

The optimized structure of the sodium complex with **L**′ is given in Figure 14. The minimal distance between protons of neighboring *tert*-butyl groups is 2.855 Å, which is again similar to the square *cone* conformation of the free ligand. In this complex, intramolecular hydrogen bonds do not exist because the $Na^+$ is octacoordinated with the oxygen atoms. Such

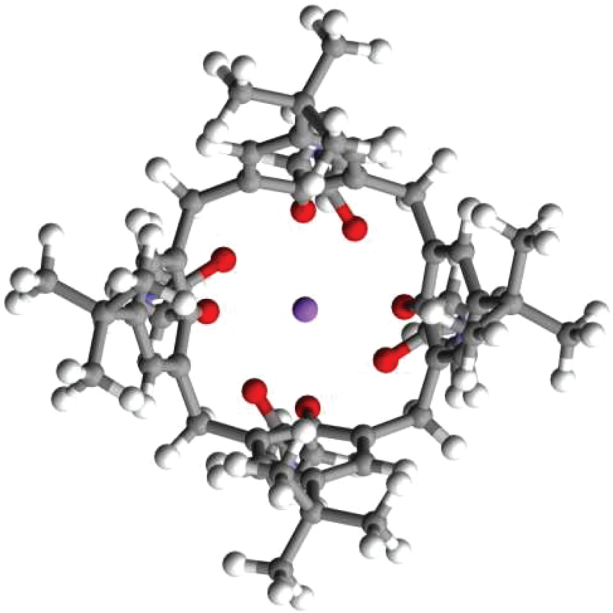

**Figure 14.** Molecular structure of the $Na^+$ complex with **L**′ optimized at the B3LYP/6-311++G(d,p) level of theory.

coordination of $Na^+$ has been noticed in the crystal structure of $[NaL]ClO_4$. NH groups are pointing outside and present free positions for the possible formation of hydrogen bonds with the solvent molecules in a fashion similar to that seen in the crystal structure of $[NaL]ClO_4$, where the NH groups are hydrogen-bonded with the perchlorate anions.

**Calculations of NMR Spectra.** A comparison between experimental and theoretical NMR chemical shifts provides practical information on the chemical structure and conformation of the investigated macrocycle and its complexes. The results of the calculations for the square *cone* conformation of calix[4]arene ($C_4$ point group; Figure 12) confirmed our initial assignation (Tables S4 and S5, Supporting Information).

**MD Simulation of Free Ligand in MeCN.** The geometry of the **L** *cone* can be represented by the distances between the opposing phenyl carbon atoms that are directly connected to the *tert*-butyl group. In that way, it can be seen (Figure 15) that,

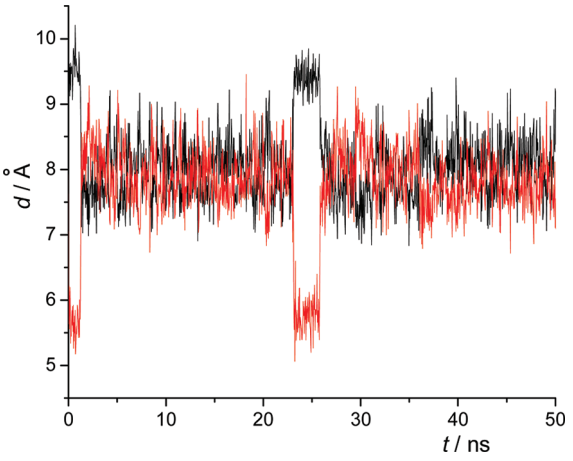


**Figure 15.** Distances between the opposing phenyl carbon atoms that are directly connected to the *tert*-butyl group during the MD simulation of **L** in MeCN.

immediately after the beginning of simulation, **L** changed the conformation from an initial square *cone*, as in the crystal structure of $NaL^+$, to a flattened *cone*, which was similar to the one obtained by crystallographic and DFT investigations.

After 1.2 ns, a molecule of MeCN entered the **L** *cone*. That was reflected in the distances between the aromatic carbon atoms, which became similar (Figure 15), making the *cone* symmetry approximately $C_4$. The MeCN methyl group pointed inside the **L** *cone*, in accordance with the solid-state structure. A similar result was observed earlier by MD simulations of systems comprising the other calixarene derivatives.[25,32] The solvent molecule in the **L**MeCN adduct left the calixarene cavity after 22 ns, resulting again in a flattened *cone* conformation of **L**. A total of 4 ns later, another MeCN molecule entered the *cone* and remained there until the end of the simulation. At the lower rim of **L**, the formation of two kinds of intramolecular NH···O═C hydrogen bonds was observed, namely, two-center and three-center ones. In the latter case, two hydrogen atoms are bound to one carbonyl oxygen atom. The number of intramolecular hydrogen bonds ranges from 0 to 3, with the average for **L** being 2.1 and that for **L**MeCN 1.5. Criteria applied for an interaction to be characterized as a hydrogen bond were that the N−H−O angle was between 100° and 180° and that the distance between nitrogen and oxygen atoms was not larger than 3.5 Å.


dx.doi.org/10.1021/ic300474s | *Inorg. Chem.* XXXX, XXX, XXX−XXX

When two or more hydrogen bonds were formed, in 52% of the cases the three-center bond was found for **L** and only 20% for **L**MeCN. A similar number and type of hydrogen bonds were observed in the crystal structures of **L** (one three-center intramolecular hydrogen bond; Figure 3a,b) and **L**MeCN (one two-center intramolecular hydrogen bond; Figure 3c). Distribution of the hydrogen-bond lengths obtained by MD simulation has a maximum between 2.8 and 2.9 Å, which is in agreement with the hydrogen bond lengths in the solid state (Table S2 and Figure S18, Supporting Information). In addition, the average structure of **L** obtained by MD simulation agrees very well with its molecular structure in the crystal. That can be taken as a corroboration of our choice of the force-field parameters.

The stabilization potential energy of the **L**MeCN species relative to **L** is −74 kJ mol$^{-1}$. If one subtracts the MeCN vaporization internal energy (30.5 kJ mol$^{-1}$)[33a] from this value, the overall stabilization effect amounts to −43.5 kJ mol$^{-1}$, which is comparable with the enthalpies of MeCN inclusion in the *tert*-butyl calix[4]arene *cone* measured by Arena et al. (−35 to −39 kJ mol$^{-1}$).[4c,d] Such a stabilization energy indicates that the **L**MeCN adduct is likely to exist in a MeCN solution of **L**, as confirmed by $^1$H NMR spectroscopy.

**MD Simulations of Complexes of L with Alkali-Metal Cations in MeCN.** MD simulation of the Li**L**$^+$ complex in MeCN was carried out. The complex was initially without a MeCN molecule included and was in a flattened *cone* conformation (less flattened than in the case of free **L**). After 62 ps of simulation, the solvent molecule entered the Li**L**$^+$ *cone* and distances between the opposing phenyl carbon atoms became approximately the same. After 4 ns, the MeCN molecule exited the Li**L**MeCN$^+$ complex, leaving the *cone* empty. In a very short period of time (180 ps), another solvent molecule entered the calixarene hydrophobic cavity. During the whole simulation (50 ns), six different MeCN molecules were found to be included in the calixarene *cone*. Throughout the periods when there was no solvent molecule bound, the calixarene *basket* showed more flexibility and streamed toward a flattened *cone* conformation. These findings can serve as an additional confirmation of the $^1$H NMR-based conclusions concerning the appearance of two forms of **L** complexes with Li$^+$, i.e., Li**L**$^+$ and Li**L**MeCN$^+$, in a MeCN solution.

When there was no MeCN molecule specifically bound in the complex, the average coordination number of the Li$^+$ cation was found to be about 6. In this case, the cation was coordinated by four phenolic oxygen atoms and on average 2.3 carbonyl oxygen atoms. On the other hand, when a MeCN molecule was included in the hydrophobic cavity, the average number of carbonyl oxygen atoms in the coordination sphere of Li$^+$ increased to 2.8, which was reflected in the energetically more favorable Li$^+$−**L** interaction in Li**L**MeCN$^+$ (−507 kJ mol$^{-1}$) compared to Li**L**$^+$ (−492 kJ mol$^{-1}$). The slight increase in the coordination number was likely due to the allosteric effect of MeCN inclusion, which reduced the flexibility of the complexed ligand.

Immediately after the beginning of the simulation of the Na**L**$^+$ complex, a MeCN molecule entered the calixarene *basket* and remained there until the end of the simulation. This result, along with the other studies conducted, confirmed the assignation of the $^1$H NMR spectra of **L** and Na$^+$ solutions at $n(Na^+)/n(\mathbf{L}) \geq 1$ condition. In other words, it corroborated the conclusion that the observed signals corresponded to the Na**L**MeCN$^+$ species. The distances between the opposing phenyl carbon atoms bound to the *tert*-butyl group were practically the same, indicating the existence of $C_4$ *cone* conformation. The Na$^+$ cation was on average coordinated by 4 phenolic and 3.3 carbonyl oxygen atoms. The latter corresponded to the time average of the structure, with all four carbonyl oxygen atoms oriented toward Na$^+$ and that with one carbonyl oxygen atom oriented toward the solvent. This was in accordance with the crystal molecular structure of Na**L**MeCN$^+$, where the Na$^+$ cation is heptacoordinated (Figure 4b). It should also be mentioned that the average cation−oxygen atom distances obtained by MD simulation were similar to those found in the crystal.

The average number of carbonyl oxygen atoms that coordinate Na$^+$ is greater than in the case of the Li**L**MeCN$^+$ complex. That can be explained by taking into account the difference in ionic radii of the free cations. Because Li$^+$ is considerably smaller than Na$^+$ [$r$(Li$^+$) = 0.76 Å; $r$(Na$^+$) = 1.02 Å for coordination number 6],[33b] it can be reasonably expected that the ligand binding sites will be more easily accommodated around the latter than the former cation. Nevertheless, the cation−calixarene interaction is weaker in the case of the Na**L**MeCN$^+$ complex (−431 kJ mol$^{-1}$) compared to Li**L**MeCN$^+$.

In the simulation of the K**L**$^+$ complex, a molecule of MeCN entered the calixarene hydrophobic cavity after 0.5 ns. During the simulation (50 ns), five different MeCN molecules entered/left the calixarene *cone*, whereby the complex without the MeCN molecule included existed for very short periods of time. The average K$^+$ coordination number was 7.9 in the case of K**L**MeCN$^+$ (3.9 carbonyl oxygens), whereas it was somewhat lower in the K**L**$^+$ complex (7.7). The higher coordination number compared to Li$^+$ and Na$^+$ can be accounted for by the reasoning similar to that described above. However, the cation−**L** interaction in K**L**MeCN$^+$ (−353 kJ mol$^{-1}$) and K**L**$^+$ (−360 kJ mol$^{-1}$) is weaker than that in the corresponding lithium and sodium complexes. The average distances between the cation and oxygen atoms of **L** obtained for K**L**MeCN$^+$ species agree with those found in the crystal structure of the K$^+$ ion complex with a similar calixarene ligand having the MeCN molecule included in the hydrophobic *basket*.[4e]

The MD simulations showed that the energy of the MeCN−calixarene interaction in **L**MeCN, Li**L**MeCN$^+$, Na**L**MeCN$^+$, and K**L**MeCN$^+$ species is almost the same and amounts to −50 kJ mol$^{-1}$.

## CONCLUSION

The comprehensive structural (solution and solid state), thermodynamic, and computational studies were undertaken in order to get a detailed insight into the reactivity of the calix[4]arene derivative **L**. Complexation of this compound with alkali-metal cations was thoroughly investigated, as was the inclusion of the MeCN molecule in the hydrophobic cavity of the free and complexed form of the ligand. On the basis of the results of the thermodynamic investigations, it was concluded that for complexation of Li$^+$, Na$^+$, and K$^+$ with **L** in MeCN, both enthalpic and entropic contributions to the corresponding reaction Gibbs energies were favorable. However, in the case of the Li$^+$ cation, the entropic contribution was dominant, whereas for Na$^+$ and K$^+$ cations, the complexation reactions were mostly enthalpically controlled. The stability constants of the complexes were determined by means of spectrophotometric, conductometric, potentiometric, and microcalorimetric titrations. The values obtained by different methods agreed very


dx.doi.org/10.1021/ic300474s | Inorg. Chem. XXXX, XXX, XXX−XXX

well, indicating their reliability. The binding affinity of **L** for $Na^+$ was found to be the highest. The selectivity of the ligand toward the $Na^+$ cation with respect to the others can be expressed as the ratio of the corresponding stability constants. From the data in Table 2, it follows that $Na^+/Li^+$ selectivity is about 7, whereas the $Na^+/K^+$ one amounts to ≈2200.

The $^1H$ NMR spectrum of **L** in deuterated acetonitrile was characterized by an existence of two signals for each of the ligand protons with unequal integrals. These signals were assigned to the free calixarene and its adduct with acetonitrile, and the equilibrium constant for the $CD_3CN$ inclusion reaction was calculated. The inclusion of the solvent molecule in the ligand hydrophobic cavity in the Na**L**$^+$ complex was found to be much more favorable compared to the free ligand. That can be explained by taking into account the fact that coordination of the $Na^+$ cation results in the preorganization of the calixarene upper-rim cavity into a rigid *cone* conformation, which provides its stronger interactions with the MeCN molecule. This conclusion was in agreement with the results of molecular simulations. Unlike Na**L**$^+$, the specific interaction of Li**L**$^+$ with MeCN is not so strong (although stronger than that with uncomplexed **L**). The reason probably lies in the more flexible conformation that calixarene adopts upon binding with $Li^+$ compared to $Na^+$. The $^1H$ NMR spectrum of **L** completely complexed by $Li^+$ in $CD_3CN$ showed two sets of signals corresponding to the species with and without the MeCN molecule included. That allowed for the determination of the equilibrium constant for the reaction of Li**L**MeCN$^+$ complex formation from Li**L**$^+$ and MeCN. By knowing this value, together with the one corresponding to the MeCN binding with the free ligand and the macroscopic $Li^+$ + **L** binding constant, it was possible to calculate the microscopic equilibrium constants for the formation of Li**L**$^+$ and Li**L**MeCN$^+$ species (Scheme 2).

The structures of **L** and its complexes with $Na^+$ and MeCN were also explored by single-crystal X-ray diffraction, as well as by DFT and MD computational studies. The conformations of **L** and its MeCN adduct in the solid state corroborate the existence of the specific MeCN−calixarene interaction observed in the MeCN solution of **L**. Crystallization of **L** from a mixture of solvents containing MeCN yielded a MeCN−calixarene supramolecular complex where the MeCN molecule is inserted in the calixarene *cone* so that the methyl group forms weak C−H···$\pi$ hydrogen bonds with the aromatic rings of the *cone*. The insertion of MeCN into the calixarene hydrophobic cavity changes its conformation from a flattened *cone* of free **L** to a regular one in **L**MeCN. Binding of $Na^+$ to **L** has a similar effect on the conformation of the ligand, as can be seen from the crystal structure of [Na**L**]$ClO_4$, where the calixarene *cone* is of $C_4$ symmetry. When MeCN was added to a solution of the sodium complex, insertion of the MeCN molecule into the ligand *cone* occurred. This yielded Na**L**MeCN$^+$ species with the *cone* conformation virtually identical with those found in both **L**MeCN and Na**L**$^+$. It therefore follows that no change of the molecular conformation is needed to allow entry of the MeCN molecule in the Na**L**$^+$ complex, whereas that is not the case for the inclusion of MeCN in **L**. This is in accordance with the more favorable inclusion of MeCN in Na**L**$^+$ compared to **L**, as observed in the solution.

Geometry optimizations and calculation of isotropic shieldings for **L** and its complexes with $Na^+$ and the MeCN molecule were performed using DFT at the B3LYP/6-311++G(d,p) level. Calculations showed that the flattened *cone* conformation ($C_2$ point group) of **L** is more favorable than the square *cone* conformation ($C_4$ point group). The structures of the **L**MeCN adduct and Na**L**$^+$ complex were found to be similar to the square *cone* conformation of free calixarene. However, in the case of **L**MeCN species, the sloping of the MeCN molecule inside the ligand *cone* caused a slight distortion from $C_4$ symmetry. The inclined position of the MeCN molecule in the cavity implied the possibility of its active movement. To investigate in more detail this movability, classical MD simulations were performed. The results indicate that free **L** and the **L**MeCN adduct coexist in the MeCN solution of the investigated macrocycle. The MeCN molecule included in the calixarene hydrophobic *cone* has only a slight effect on the structure of the lower-rim hydrophilic cavity and, consequently, on its metal-ion-binding ability. That can be seen from the average number of intramolecular NH···O═C hydrogen bonds present in **L** (2.1) compared to **L**MeCN (1.5). In the M**L**$^+$ complexes, the ligand is in the appropriate square *cone* conformation to bind the MeCN molecule, allowing it to easily enter the hydrophobic cavity. However, the dynamics of MeCN binding by **L** rather strongly depends on the cation comprising the complex. In Na**L**$^+$, the MeCN molecule remains in the cavity until the end of the simulation (50 ns), while in the case of Li**L**$^+$ and K**L**$^+$, it frequently enters and leaves the cavity. To test the hypothesis that preorganization of the calixarene basket into the square *cone* conformation is of great importance for its filling with the MeCN molecule, we have performed a MD simulation in which the distances between the opposing phenyl carbon atoms that are directly connected to the *tert*-butyl groups were restricted to those in the Na**L**$^+$ complex. It was found that the MeCN molecule immediately enters the calixarene *cone* and remains there during most of the simulation time. From the above considerations, it can be concluded that cation binding by **L** has a rather strong allosteric effect on inclusion of the MeCN molecule in the calixarene *cone*.[25] That, in turn, has an important impact on the solution thermodynamic stability of the metal-ion complexes with the investigated macrocycle.

## ■ ASSOCIATED CONTENT

### Ⓢ Supporting Information

X-ray crystallographic data in CIF format, ORTEP plots and packing diagrams, experimental and calculated $^1H$ and $^{13}C$ NMR chemical shifts of compound **L**, temperature dependence of $^1H$ NMR spectra of **L** in $CDCl_3$ and $CD_3CN$, results of $^1H$ NMR titrations of **L** with $LiClO_4$, $NaClO_4$ and $KClO_4$ in $CD_3CN$ and $^1H$ NMR titrations of **L** and [Na**L**]$ClO_4$ with MeCN in $CDCl_3$, additional results of spectrophotometric, conductometric, and microcalorimetric titrations, and additional results of MD simulations. This material is available free of charge via the Internet at http://pubs.acs.org.

## ■ AUTHOR INFORMATION

### Corresponding Author

*E-mail: vtomisic@chem.pmf.hr.

### Notes

The authors declare no competing financial interest.

## ■ ACKNOWLEDGMENTS

This work was supported by the Ministry of Science, Education and Sports of the Republic of Croatia (Projects 119-1191342-2960, 119-1193079-3069, and 098-0982904-2912).

## REFERENCES


(1) (a) Gutsche, C. D. *Calixarenes: An Introduction*, 2nd ed.; The Royal Society of Chemistry: Cambridge, U.K., 2008. (b) *Calixarenes 2001*; Asfari, Z., Böhmer, V., Harrowfield, J., Vicens, J., Eds.; Kluwer Academic Publishers: Dordrecht, The Netherlands, 2001. (c) *Calixarenes in the Nanoworld*; Vicens, J., Harrowfield, J., Eds.; Springer: Dordrecht, The Netherlands, 2001. (d) Danil de Namor, A. F.; Cleverley, R. M.; Zapata-Ormachea, M. L. *Chem. Rev.* **1998**, *98*, 2495−2525. (e) Böhmer, V. *Angew. Chem., Int. Ed. Engl.* **1995**, *34*, 713−745.

(2) (a) Schüle, D. T.; Peters, J. A.; Schatz, J. *Coord. Chem. Rev.* **2011**, *255*, 2727−2745. (b) Mokhtari, B.; Pourabdollah, K.; Dalali, N. *J. Inclusion Phenom. Macrocyclic Chem.* **2011**, *69*, 1−55. (c) Sliwa, W.; Girek, T. *J. Inclusion Phenom. Macrocyclic Chem.* **2010**, *66*, 15−41. (d) Creaven, B. S.; Donlon, D. F.; McGinley, J. *Coord. Chem. Rev.* **2009**, *253*, 893−962. (e) Sliwa, W. *J. Inclusion Phenom. Macrocyclic Chem.* **2005**, *52*, 13−37. (f) Ludwig, R.; Dzung, N. T. K. *Sensors* **2002**, *2*, 397−416.

(3) (a) Matthews, S. E.; Beer, P. D. *Supramol. Chem.* **2005**, *17*, 411−435. (b) Lhoták, P. *Top. Curr. Chem.* **2005**, *255*, 65−95. (c) Matthews, S. E.; Beer, P. D. In *Calixarenes 2001*; Asfari, Z., Böhmer,V., Harrowfield, J., Vicens, J., Eds.; Kluwer Academic Publishers: Dordrecht, The Netherlands, 2001; pp 421−439. (d) Hamdi, A.; Abidi, R.; Vicens, J. *J. Inclusion Phenom. Macrocyclic Chem.* **2008**, *60*, 193−196. (e) Okunola, O. A.; Seganish, J. L.; Salimian, K. J.; Zavaliy, P. Y.; Davis, J. T. *Tetrahedron* **2007**, *63*, 10743−10750. (f) Sun, X. H.; Li, W.; Xia, P. F.; Luo, H.; Wei, Y.; Wong, M.; Cheng, Y.; Shuang, S. *J. Org. Chem.* **2007**, *72*, 2419−2426.

(4) (a) Arduini, A.; Pochini, A.; Secchi, A.; Ugozzoli, F. In *Calixarenes 2001*; Asfari, Z., Böhmer, V., Harrowfield, J., Vicens, J., Eds.; Kluwer Academic Publishers: Dordrecht, The Netherlands, 2001; pp 457−475. (b) Cuřínová, P.; Pojarová, M.; Budka, J.; Lang, K.; Stibor, I.; Lhoták, P. *Tetrahedron* **2010**, *66*, 8047−8050. (c) Arena, G.; Contino, A.; Longo, E.; Spoto, G.; Arduini, A.; Pochini, A.; Secchi, A.; Massera, C.; Ugozzolli, F. *New J. Chem.* **2004**, *28*, 56−61. (d) Arena, G.; Continoa, A.; Magrì, A.; Sciottoa, D.; Arduini, A.; Pochini, A.; Secchi, A. *Supramol. Chem.* **2001**, *13*, 379−386. (e) Arduini, A.; Giorgi, G.; Pochini, A.; Secchi, A.; Ugozzolli, F. *Tetrahedron* **2001**, *57*, 2411−2417. (f) Smirnov, S.; Sidorov, V.; Pinkhassik, V.; Havlicek, J.; Stibor, I. *Supramol. Chem.* **1997**, *8*, 187−196. (g) Wang, J.; Bodige, S. G.; Watson, W. H.; Gutsche, C. D. *J. Org. Chem.* **2000**, *65*, 8260−8263.

(5) (a) Nomura, E.; Takagaki, M.; Nakaoka, C.; Uchida, M.; Taniguchi, H. *J. Org. Chem.* **1999**, *64*, 3151−3156. (b) Frkanec, L.; Višnjevac, A.; Kojić-Prodić, B.; Žinić, M. *Chem.—Eur. J.* **2000**, *6*, 442−453. (c) Cho, Y. L.; Rudkevich, D. M.; Shivanyuk, A.; Rissanen, K.; Rebek, J., Jr. *Chem.—Eur. J.* **2000**, *6*, 3788−3796. (d) Mareque Rivas, J.; Schwalbe, C. H.; Lippard, S. J. *Proc. Natl. Acad. Sci. U.S.A.* **2001**, *98*, 9478−9483. (e) Stibor, I.; Ružičkova, M.; Krátký, R.; Vindyš, M.; Havlíček, J.; Pinkhassik, E.; Lhoták, P.; Mustafina, A. R.; Morozova, Y. E.; Kazakova, E. Kh.; Gubskaya, V. P. *Collect. Czech. Chem. Commun.* **2001**, *66*, 641−662. (f) No, K.; Lee, J. H.; Yang, S. H.; Yu, S. H.; Cho, M. H.; Kim, M. J.; Kim, J. S. *J. Org. Chem.* **2002**, *67*, 3165−3168. (g) No, K.; Lee, J. H.; Yang, S. H.; Noh, K. H.; Lee, S. W.; Kim, J. S. *Tetrahedron* **2003**, *59*, 2403−2407. (h) Xu, H.; Kinsel, G. R.; Zhang, J.; Li, M. *Tetrahedron* **2003**, *59*, 5837−5848. (i) Tomišić, V.; Galić, N.; Bertoša, B.; Frkanec, L.; Simeon, V.; Žinić, M. *J. Inclusion Phenom. Macrocyclic Chem.* **2005**, *53*, 263−268. (j) Baldini, L.; Sansone, F.; Scaravelli, F.; Casnati, A.; Ungaro, R. *Supramol. Chem.* **2010**, *22*, 776−788. (k) Požar, J.; Preočanin, T.; Frkanec, L.; Tomišić, V. *J. Solution Chem.* **2010**, *39*, 835−848. (l) Galić, N.; Burić, N.; Tomaš, R.; Frkanec, L.; Tomišić, V. *Supramol. Chem.* **2011**, *23*, 389−397.

(6) (a) Danil de Namor, A. F.; Hutcherson, R. G.; Sueros Velarde, F. J.; Zapata-Ormachea, M. L.; Pulcha Salazar, L. E.; Al Jammaz, I.; Al Rawi, N. *Pure Appl. Chem.* **1998**, *70*, 769−778. (b) Danil de Namor, A. F. In *Calixarenes 2001*; Asfari, Z., Böhmer, V., Harrowfield, J., Vicens, J., Eds.; Kluwer Academic Publishers: Dordrecht, The Netherlands, 2001; pp 346−364. (c) Arnaud-Neu, F.; McKervey, M. A.; Schwing-Weill, M.-J. In *Calixarenes 2001*; Asfari, Z., Böhmer, V., Harrowfield, J., Vicens, J., Eds.; Kluwer Academic Publishers: Dordrecht, The Netherlands, 2001; pp 385−406.

(7) (a) Danil de Namor, A. F.; Apaza de Sueros, N.; McKervey, M. A.; Barrett, G.; Arnaud-Neu, F.; Schwing-Weill, M. J. *J. Chem. Soc., Chem. Commun.* **1991**, *21*, 1546−1548. (b) Bonechi, C.; Donati, A.; Martini, S.; Rossi, C.; Arduini, A.; Pochini, A.; Lonetti, B.; Baglioni, P. *J. Phys. Chem. B* **2004**, *108*, 7603−7610.

(8) (a) Danil de Namor, A. F.; Chahine, S.; Castellano, E. E.; Piro, O. E. *J. Phys. Chem. A* **2005**, *109*, 6743−6751. (b) Danil de Namor, A. F.; Gil, E.; Llosa Tanco, M. A.; Pacheco Tanaca, D. A.; Pulcha Salazar, L. E.; Schulz, R. A.; Wang, J. *J. Phys. Chem.* **1995**, *99*, 16781−16785. (c) Danil de Namor, A. F.; Zapata-Ormachea, M. L.; Hutcherson, R. G. *J. Phys. Chem. B* **1999**, *103*, 366−371. (d) Danil de Namor, A. F.; Chahine, S.; Kowalska, D.; Castellano, E. E.; Piro, O. E. *J. Am. Chem. Soc.* **2002**, *124*, 12824−12836. (e) Danil de Namor, A. F.; Aparacio-Aragon, W. B.; Goitia, M. T.; Castal, R. *Supramol. Chem.* **2004**, *16*, 423−433.

(9) Armarego, W. L. F.; Chai, C. L. L. *Purification of Laboratory Chemicals*, 6th ed.; Butterworth-Heinemann (Elsevier): Oxford, U.K., 2009.

(10) Arnaud-Neu, F.; Fanni, S.; Guerra, L.; McGregor, W.; Ziat, K.; Schwing-Weill, M.-J.; Barrett, G.; McKervey, M. A.; Marrs, D.; Seward, E. M. *J. Chem. Soc., Perkin Trans. 2* **1995**, 113−118.

(11) (a) Gampp, H.; Maeder, M.; Meyer, C. J.; Zuberbühler, A. D. *Talanta* **1985**, *32*, 95−101. (b) Gampp, H.; Maeder, M.; Meyer, C. J.; Zuberbühler, A. D. *Talanta* **1985**, *32*, 251−264. (c) Maeder, M.; Zuberbühler, A. D. *Anal. Chem.* **1990**, *62*, 2220−2224.

(12) Gans, P.; Sabatini, A.; Vacca, A. *Talanta* **1996**, *43*, 1739−1753.

(13) Briggner, L. E.; Wadsö, I. J. *Biochem. Biophys. Methods* **1991**, *22*, 101−118.

(14) Oxford Diffraction. *CrysAlis CCD and CrysAlis RED*, version 1.170; Oxford Diffraction Ltd.: Wroclaw, Poland, 2003.

(15) Sheldrick, G. M. *Acta Crystallogr., Sect. A* **2008**, *64*, 112−122.

(16) Farrugia, L. J. *J. Appl. Crystallogr.* **1999**, *32*, 837−838.

(17) Allen, F. H. *Acta Crystallogr., Sect. B* **2002**, *58*, 380−388.

(18) Stilinović, V.; Kaitner, B. *Acta Crystallogr., Sect. A* **2010**, *66*, 441−445.

(19) Frisch, M. J.; Trucks, G. W.; Schlegel, H. B.; Scuseria, G. E.; Robb, M. A.; Cheeseman, J. R.; Montgomery, J. A., Jr.; Vreven, T.; Kudin, K. N.; Burant, J. C.; Millam, J. M.; Iyengar, S. S.; Tomasi, J.; Barone, V.; Mennucci, B.; Cossi, M.; Scalmani, G.; Rega, N.; Petersson, G. A.; Nakatsuji, H.; Hada, M.; Ehara, M.; Toyota, K.; Fukuda, R.; Hasegawa, J.; Ishida, M.; Nakajima, T.; Honda, Y.; Kitao, O.; Nakai, H.; Klene, M.; Li, X.; Knox, J. E.; Hratchian, H. P.; Cross, J. B.; Bakken, V.; Adamo, C.; Jaramillo, J.; Gomperts, R.; Stratmann, R. E.; Yazyev, O.; Austin, A. J.; Cammi, R.; Pomelli, C.; Ochterski, J. W.; Ayala, P. Y.; Morokuma, K.; Voth, G. A.; Salvador, P.; Dannenberg, J. J.; Zakrzewski, V. G.; Dapprich, S.; Daniels, A. D.; Strain, M. C.; Farkas, O.; Malick, D. K.; Rabuck, A. D.; Raghavachari, K.; Foresman, J. B.; Ortiz, J. V.; Cui, Q.; Baboul, A. G.; Clifford, S.; Cioslowski, J.; Stefanov, B. B.; Liu, G.; Liashenko, A.; Piskorz, P.; Komaromi, I.; Martin, R. L.; Fox, D. J.; Keith, T.; Al-Laham, M. A.; Peng, C. Y.; Nanayakkara, A.; Challacombe, M.; Gill, P. M. W.; Johnson, B.; Chen, W.; Wong, M. W.; Gonzalez, C.; Pople, J. A. *Gaussian 03*, revision D.01; Gaussian, Inc.: Wallingford, CT, 2004.

(20) (a) Miertuš, S.; Scrocco, E.; Tomasi, J. *Chem. Phys.* **1981**, *55*, 117−129. (b) Tomasi, J.; Persico, M. *Chem. Rev.* **1994**, *94*, 2027−2094.

(21) (a) Cancès, E.; Mennucci, B. *J. Math. Chem.* **1998**, *23*, 309−326. (b) Cancès, E.; Mennucci, B.; Tomasi, J. *J. Chem. Phys.* **1997**, *107*, 3032−3041. (c) Mennucci, B.; Cancès, E.; Tomasi, J. *J. Phys. Chem. B* **1997**, *101*, 10506−10517. (d) Mennucci, B.; Cammi, R.; Tomasi, J. *J. Chem. Phys.* **1998**, *109*, 2798−2807.

(22) (a) Cammi, R.; Mennucci, B.; Tomasi, J. *J. Chem. Phys.* **1999**, *110*, 7627−7638. (b) Cammi, R. *J. Chem. Phys.* **1998**, *109*, 3185−3196.

(23) Hess, B.; Kutzner, C.; van der Spoel, D.; Lindahl, E. *J. Chem. Theory Comput.* **2008**, *4*, 435−447.

(24) Jorgensen, W. L.; Maxwell, D. S.; Tirado-Rives, J. *J. Am. Chem. Soc.* **1996**, *118*, 11225−11236.

(25) de Araujo, A. S.; Piro, O. E.; Castellano, E. E.; Danil de Namor, A. F. *J. Phys. Chem. A* **2008**, *112*, 11885−11894.



dx.doi.org/10.1021/ic300474s | *Inorg. Chem.* XXXX, XXX, XXX−XXX

(26) Swope, W. C.; Andersen, H. C.; Berens, P. H.; Wilson, K. R. J. *J. Chem. Phys.* **1982**, *76*, 637−649.
(27) (a) Darden, T.; York, D.; Pedersen, L. J. *Chem. Phys.* **1993**, *98*, 10089−10092. (b) Essmann, U.; Perera, L.; Berkowitz, M. L.; Darden, T.; Lee, H.; Pedersen, L. G. *J. Chem. Phys.* **1995**, *103*, 8577−8593.
(28) (a) Nosé, S. *Mol. Phys.* **1984**, *52*, 255−268. (b) Hoover, W. G. *Phys. Rev. A* **1985**, *31*, 1695−1697.
(29) Martyna, G. J.; Tuckerman, M. E.; Tobias, D. J.; Klein, M. L. *Mol. Phys.* **1996**, *87*, 1117−1157.
(30) Ugozzoli, F.; Andreetti, G. *J. Inclusion Phenom. Mol. Recognit. Chem.* **1992**, *13*, 337−348.
(31) Bäckman, P.; Bastos, M.; Hallén, D.; Lönnbro, P.; Wadsö, I. *J. Biochem. Biophys. Methods* **1994**, *28*, 85−100.
(32) Guilbaud, P.; Varnek, A.; Wipff, G. *J. Am. Chem. Soc.* **1993**, *115*, 8298−8312.
(33) *CRC Handbook of Chemistry and Physics*, 87th ed.; Lide, D. R., Ed.; CRC Press: Boca Raton, FL, 2006; (a) pp 6−98; (b) pp 12-11 and 12-12.

## ■ NOTE ADDED AFTER ASAP PUBLICATION

Due to a production error Table 2 was incorrect in the version published ASAP May 9, 2012; the correct version reposted May 11, 2012.


dx.doi.org/10.1021/ic300474s | *Inorg. Chem.* XXXX, XXX, XXX−XXX